Astron. Astrophys. 356, 1119–1135 (2000)

ASTRONOMY AND ASTROPHYSICS

Astrometric radial velocities

II. Maximum-likelihood estimation of radial velocities in moving clusters⋆

Lennart Lindegren, Søren Madsen, and Dainis Dravins

Lund Observatory, Box 43, SE-22100 Lund (lennart, soren, dainis@astro.lu.se)

Received 1 September 1999 / Accepted 10 February 2000

Abstract. Accurate proper motions and trigonometric parallaxes of stars in nearby open clusters or associations permit to determine their space motions relative to the Sun, without using spectroscopy for their radial-velocity component. This assumes that the member stars share the same mean velocity vector, apart from a (small) random velocity dispersion. We present a maximum-likelihood formulation of this problem and derive an algorithm for estimating the space velocity and internal velocity dispersion of a cluster using astrometric data only. As a by-product, kinematically improved parallaxes and distances are obtained for the individual cluster stars. The accuracy of the method, its robustness, and its sensitivity to internal velocity fields, are studied through Monte Carlo simulations, using the Hyades as a test case. From Hipparcos data we derive the centroid velocity and internal velocity dispersion of the Hyades cluster. The astrometric radial velocities are obtained with a standard error of 0.47 km s^{-1} for the cluster centroid, increasing to about 0.68 km s^{-1} for the individual stars due to their peculiar velocities. If known binaries are removed, this improves to 0.60 km s^{-1}.

Key words: methods: data analysis – techniques: radial velocities – astrometry – stars: distances – stars: kinematics – Galaxy: open clusters and associations: general

1. Introduction

In a previous paper (Dravins et al. 1999, hereafter Paper I) three methods were described by which stellar radial velocities can be determined astrometrically, i.e. from geometric measurements independent of spectroscopy. Such *astrometric radial velocities* are of interest as they allow to disentangle the space motions of the stars from other astrophysical phenomena causing spectroscopic line shifts, such as internal motions in stellar atmospheres and gravitational redshift. In normal stars such shifts are typically less than 1 km s^{-1}. A corresponding accuracy is needed in the astrometric radial velocity to permit useful comparison with spectroscopic data. Two of the methods outlined in Paper I use the progressively changing parallax or proper motion of a star to infer its motion relative to the Sun. Reaching < 1 km s^{-1} accuracy with these methods requires astrometric observations on the microarcsec accuracy level, currently unavailable but likely to be achieved in future space astrometry programmes.

The third method is based on the changing angular extent of a star cluster as it approaches or recedes from the Sun: the relative rate of apparent contraction equals the relative change in distance. Since the distance is known from trigonometric parallaxes, the radial velocities follow. Only this method can provide sub-km s^{-1} radial velocity estimates from existing astrometric data. In the present paper we develop a maximum-likelihood (ML) algorithm, first described by Dravins et al. (1997), for estimating the space velocity vector and other kinematic parameters of a cluster. These results can then be used to estimate the radial velocities of individual member stars, simply by projecting the cluster velocity vector onto their lines of sight.

An overview of the method is presented in Sect. 2, followed by the precise mathematical formulation in Sect. 3. Details of the practical implementation are given in Appendix A. The validity of the method is studied in Sect. 4 by means of Monte Carlo simulations, and in Sect. 5 we apply the method to the Hyades cluster as observed by Hipparcos. It is concluded that the method can indeed yield accurate results under realistic assumptions, although special procedures are needed to correctly estimate the internal velocity dispersion of the cluster and the accuracies of the estimated parameters. In a subsequent paper (Paper III: Madsen et al., in preparation) the method is systematically applied to Hipparcos observations of nearby open star clusters.

A by-product of the moving-cluster method is that the distance estimates to the individual cluster stars may be significantly improved compared with the original parallax measurements. As discussed in Paper I (Sect. 6.3), these 'kinematically improved parallaxes' can be understood as resulting from a combination of trigonometric and kinematic distance information, where kinematic distances follow from the observed proper motions and the derived cluster velocity.

2. Overview of the method

The aim of the present method is to estimate the radial velocities of the stars in a moving cluster, based exclusively on

⋆ Based (in part) on observations by the ESA Hipparcos satellite

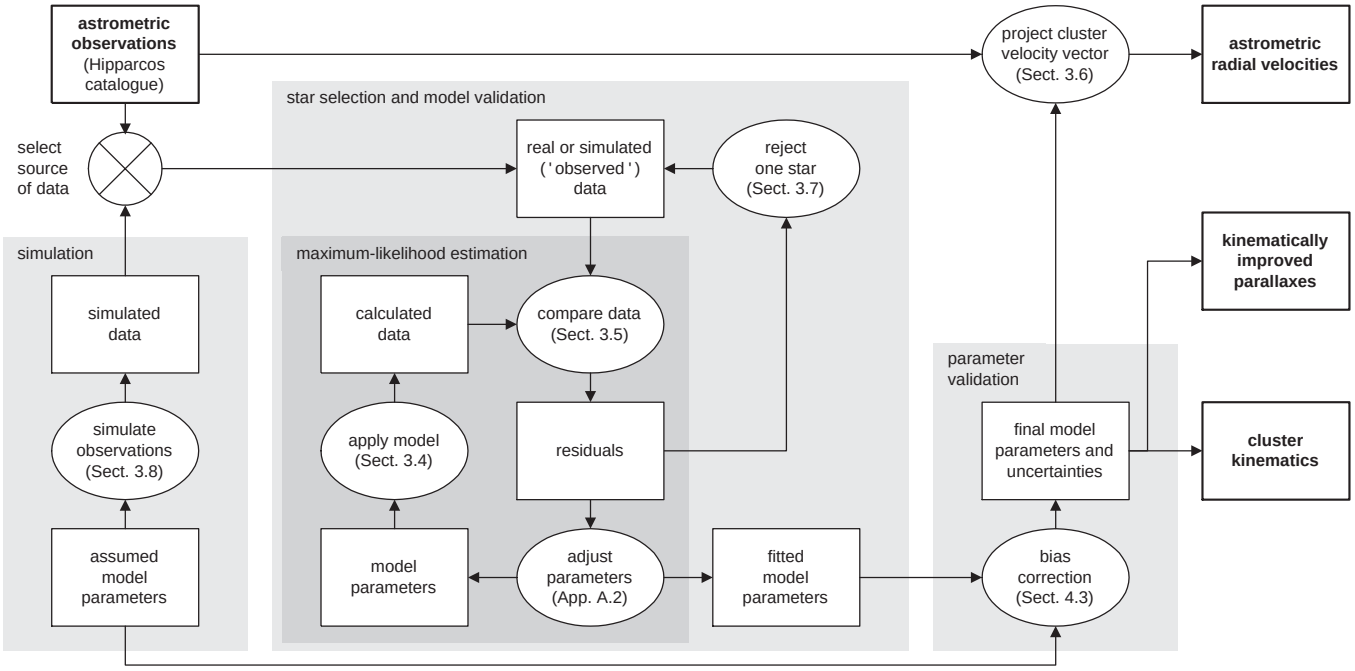

Fig. 1. Flow diagram for the computation of astrometric radial velocities and kinematically improved parallaxes of a moving cluster. The section where each computational step is described is indicated on the chart.

astrometric data (mainly proper motions and trigonometric parallaxes). In effect, it reverses the well-known 'moving-cluster method' (Binney & Merrifield 1998) in which the distances to the stars in a moving cluster are derived from the proper motions and (spectroscopic) radial velocities: if instead the distances are known from the trigonometric parallaxes, the radial velocities follow. The classical application of the moving-cluster method, e.g. by van Bueren (1952), proceeds in three steps: firstly, the convergent point is located from the directions of the proper motions; secondly, the common space velocity (in km s^{-1}) of the stars is derived from the spectroscopic radial velocities using the adopted convergent point; and finally the distances to the individual stars are computed from their observed proper motions and the adopted space velocity. The resulting distance estimates are referred to as 'kinematic distances' or 'kinematic parallaxes', as they are based on the kinematic parameters of the cluster. Murray & Harvey (1976) gave a rigorous formulation of the technique, in which the conventional division into the three steps mentioned above was replaced by a simultaneous least-squares solution for the kinematic parameters and the (kinematic) parallax of each individual star.

The overall approach of our method is similar to that of Murray & Harvey (1976), in that a simultaneous solution is made for the kinematic parameters of the cluster and the individual parallaxes. The main differences with respect to the classical formulation are: (1) spectroscopic radial velocities are *not* used as input to the solution; (2) trigonometric parallaxes *are* on the other hand used as input; (3) the kinematic model of the cluster is refined by including an internal velocity dispersion and a possible first-order velocity field. In addition, a special procedure for rejection of outliers (e.g. non-member stars) is incorporated and extensive Monte Carlo simulations are used to validate the results.

Both the classical moving-cluster method and the present method can be regarded as special cases of the more general 'statistical parallax' method (Hawley et al. 1986; Strugnell et al. 1986; Popowski & Gould 1998; Narayanan & Gould 1999a), in which distances and kinematic parameters may be derived from a combination of astrometric, spectroscopic, and photometric data.

A detailed description of our method is given in the following sections and in Appendix A. The flow diagram for the computations is shown in Fig. 1, including references to the sections of this paper where the different steps are described. The most important parts of the procedure are summarised below.

Input data and initial stellar sample: The present method assumes that a provisional sample of stars likely to be members of the cluster has been identified and that accurate astrometric data (positions, proper motions and trigonometric parallaxes) are available for this sample. The initial sample may be defined by means of classic kinematic and photometric criteria, e.g. as described by Platais et al. (1998).

Maximum-likelihood estimation: At the core of the computation is the maximum-likelihood (ML) estimation algorithm, which fits the parameters of the cluster model to the observed astrometric data. The model parameters are, usually, the common space velocity vector of the cluster, the internal velocity dispersion, and the distances to the individual stars. The output consists of the fitted (estimated) model parameters with their estimated uncertainties (standard errors).

Star selection and model validation: The ML algorithm assumes that the observational data conform to the statistical descriptions that are part of the model. Because the model is restricted to the cluster itself, this assumption is not valid for non-member stars. Moreover, some member stars (in particular binaries) may have deviating motions that are not included in the statistical modelling of the cluster. Residuals of the fit are used to assess the validity of the model as a whole and its applicability to the individual stars. Stars with large residuals do not conform to the model and are therefore rejected.

Simulation: The procedures above can be applied not only to observed astrometric values (e.g. from the Hipparcos Catalogue), but also to simulated data. The simulation starts with the cluster model and assumed model parameters, from which the 'true' (error-free) astrometric data are computed. Adding Gaussian measurement noise according to the assumed standard errors of the observations finally gives the simulated astrometric data. Contaminating field stars or anomalous velocity distributions can be included.

Parameter validation: The simulated observations are used to validate the ML estimation procedure: the assumed parameters should, ideally, be recovered by the estimation. Because of the added measurement noise this will at best happen as the mean result of many simulation/estimation experiments. The general technique to study properties of an estimation procedure by repeated simulation experiments is known as Monte Carlo simulation (Press et al. 1992). It is particularly important to find out whether the estimated parameters are systematically different from the assumed ones, i.e. if they are biased. In our case a significant bias was found in the ML estimation of the internal velocity dispersion, and a special procedure was devised to circumvent this effect. Monte Carlo simulations are also used to determine the uncertainties of the estimated parameters.

End products: The final model parameters, corrected for bias if necessary, provide a kinematic characterisation of the cluster as well as kinematically improved individual distances to the member stars. Projecting the common cluster velocity vector onto the line of sight of each star provides an estimate of the star's radial velocity. The error of the resulting astrometric radial velocity has two parts: a (systematic) part which derives from the estimation error of the cluster velocity vector, and a (random) part due to the peculiar velocity of the star.

3. Mathematical formulation

3.1. The precise definition of 'radial velocity'

When aiming at sub-km s^{-1} accuracy levels it becomes necessary to consider the exact meaning of the term 'radial velocity'. Spectroscopically, the measured quantity is the Doppler shift $z = (\lambda - \lambda_0)/\lambda_0$, where λ is the observed wavelength and λ_0 the rest-frame wavelength. We assume that this shift has been corrected for local effects such as the observer's motion relative to the Solar System Barycentre. Even then, the quantity z depends not only on the radial component of the star's velocity, but also on the transverse Doppler shift, gravitational redshift, gas motions in the stellar atmosphere, conventions concerning the adopted reference frames, and possibly other effects unknown to the observer. Since the precise interpretation of z in terms of stellar motion is thus model-dependent, we have proposed (Lindegren et al. 1999) that the term 'radial-velocity measure' is used for the quantity cz, and that this (well-defined) quantity should be regarded as the proper result of a spectroscopic measurement.

The above approach to the interpretation of lineshift measurements is conceptually rather different from the traditional way in which radial velocities are determined. The aim of the latter is (usually) to determine in some sense the 'true' radial components of the space motions of the stars, by removing all other sources of spectroscopic shifts. This can be done, at least for solar-type stars and up to a certain degree, through comparison with the solar spectrum, directly or indirectly via minor planets. The pioneering efforts by Griffin et al. (1988) and Gunn et al. (1988) to obtain accurate radial velocities for stars in the Hyades cluster may be cited as an example of this classical approach. We think, however, that current and future spectroscopic measurements of much higher accuracy will require a more stringent definition, in which the observable quantity (represented by the radial-velocity measure cz) is clearly separated from its physical interpretation.

The determination of astrometric radial velocities is not affected by factors such as the transverse Doppler effect and gravitational redshift. Nevertheless we need to state explicitly what we mean by radial velocity, in order to compare our astrometric results with spectroscopic determinations. The main point to consider is the light-time effects due to the finite speed of light. As the star moves through space, the time interval from light emission at the object (t_0) to the arrival at the solar system barycentre (t_1) changes, and the corresponding stretching or compression of the time scale naturally affects the observations. Rigorous treatment of this problem is beyond the present paper. The residual effect is however very small provided a single time scale (such as t_1) is consistently used to describe the phenomena. Since proper motions are defined as the time derivatives of direction with respect to t_1 ($\boldsymbol{\mu} = \mathrm{d}\boldsymbol{r}/\mathrm{d}t_1$, where $\boldsymbol{r} = \boldsymbol{b}/|\boldsymbol{b}|$ is the barycentric direction to the star) we adopt the convention that the (astrometric) radial velocity is defined as $v_r = \mathrm{d}|\boldsymbol{b}|/\mathrm{d}t_1$. In the absence of relativistic effects this is related to the Doppler shift by $v_r = cz/(1+z)$.

3.2. The maximum-likelihood method

The maximum-likelihood (ML) method is a well-known technique for parameter estimation described in most textbooks on probability theory and statistics (Kendall & Stuart 1979; Casella & Berger 1990). The following brief introduction provides some of the mathematical framework, notations and terminology required for subsequent sections.

Application of the ML estimation method requires that the observed quantities (*observables* – in our case the astrometric data) are modelled as random variables whose probability density function (pdf) depends on a finite set of *model parameters*. The model describes both the physical object itself, including

for instance random motions in the cluster, and the process of observation, i.e. measurement noise. The complete set of observables in a given estimation problem may be represented by the multidimensional variable (vector) $\boldsymbol{a}$. Similarly, the set of model parameters makes up the vector $\boldsymbol{\theta}$. Mathematically speaking, the model is fully specified by the function $p(\boldsymbol{a}|\boldsymbol{\theta})$, which is the pdf of the random variable $\boldsymbol{a}$ for given model parameters $\boldsymbol{\theta}$.

In the following we use diacritic marks to distinguish between different realisations (or versions) of the same random variable. For the generic variable x we use $\overline{x}$ to denote the true value, $\widetilde{x}$ the observed (or simulated) value, and $\widehat{x}$ the estimated value. A summary of notations is given in Appendix B.

The observations provide a unique realisation $\widetilde{\boldsymbol{a}}$ of the random variable $\boldsymbol{a}$. The problem is to find the 'best' estimate of $\boldsymbol{\theta}$ consistent with the observed data. We use the principle of maximum likelihood to obtain this estimate. The likelihood function is defined as $L(\boldsymbol{\theta}) = p(\widetilde{\boldsymbol{a}}|\boldsymbol{\theta})$ and the ML estimate $\widehat{\boldsymbol{\theta}}$ is the set of parameters maximising the likelihood or, equivalently, the log-likelihood function $\mathcal{L}(\boldsymbol{\theta}) = \ln L(\boldsymbol{\theta})$.

The curvature of $\mathcal{L}(\boldsymbol{\theta})$ in the vicinity of its maximum is a measure of the sharpness (precision) of the ML estimate. Statistical theory provides an estimate of the covariance of $\widehat{\boldsymbol{\theta}}$ in the form of a lower bound, known as the Cramér–Rao inequality (Kendall & Stuart 1979). Subject to regularity conditions this bound can be written, for the vector-valued parameter $\boldsymbol{\theta}$,

$$\mathrm{Cov}(\widehat{\boldsymbol{\theta}}) \geq \boldsymbol{V} \equiv -\left[\mathrm{E}\left(\frac{\partial^2 \mathcal{L}(\boldsymbol{\theta})}{\partial\boldsymbol{\theta}\,\partial\boldsymbol{\theta}'}\right)\right]^{-1}_{\boldsymbol{\theta}\,=\,\widehat{\boldsymbol{\theta}}} \tag{1}$$

(Silvey 1970). Here E is the statistical expectation operator and the prime denotes matrix transposition. Although Eq. (1) formally only provides a lower bound to the covariance, it is in practice often quite accurate. However, it is recommended that its validity is always checked by means of Monte Carlo simulations (Sect. 4).

A complete formulation of the moving-cluster problem thus requires specification of the model parameters ($\boldsymbol{\theta}$), the observables ($\boldsymbol{a}$), and the probability density function $p(\boldsymbol{a}|\boldsymbol{\theta})$. Additionally, the mathematical formulation includes *auxiliary data* which are regarded as fixed, i.e. known a priori, or with sufficient accuracy that their uncertainties need not be taken into account in the estimation process. These include in our case the positions of the stars, the standard errors of the observed proper motions and parallaxes, and the correlation coefficients.

3.3. Cluster model parameters

The stars in a cluster are distinguished by the subscript i running from 1 to n, the number of stars considered. The kinematic state of the cluster is completely specified by the position $\boldsymbol{b}_i$ and velocity $\boldsymbol{v}_i$ of each star relative to the solar system barycentre. The cluster model provides a parametrised statistical description of $(\boldsymbol{b}_i, \boldsymbol{v}_i, i = 1 \ldots n)$.

The three-dimensional position (in pc) of a star can be written $\boldsymbol{b}_i = \boldsymbol{r}_i(1000/\pi_i)$, where $\boldsymbol{r}_i$ is the direction (unit vector) towards the star and π_i the parallax in mas. We regard $\boldsymbol{r}_i$ as error-free, i.e. belonging to the category of auxiliary data, and π_i as a parameter of the model. The n parallaxes of the cluster constitute a vector $\boldsymbol{\pi}$ which is part of the general parameter vector $\boldsymbol{\theta}$.

Let $\boldsymbol{v}_0$ be the centroid velocity, i.e. the mean velocity of the cluster member stars. The equatorial Cartesian components of $\boldsymbol{v}_0$ constitute three more elements of the parameter vector $\boldsymbol{\theta}$.

The astrometric measurements are accurate enough to detect the deviations of the individual velocities from the centroid velocity, i.e. the tangential components of the peculiar velocities $\boldsymbol{\eta}_i = \boldsymbol{v}_i - \boldsymbol{v}_0$. Thus, a statistical description of the peculiar velocities is needed, in the form of a parametrised pdf for $\boldsymbol{\eta}_i$. We assume that the peculiar motions are Maxwellian (i.e., Gaussian in the rectangular components), and thus fully described by a dispersion tensor $\boldsymbol{S}$. We take this to be isotropic and independent of stellar mass and position in the cluster:

$$\boldsymbol{S} = \begin{bmatrix} \sigma_v^2 & 0 & 0 \\ 0 & \sigma_v^2 & 0 \\ 0 & 0 & \sigma_v^2 \end{bmatrix} . \tag{2}$$

The internal velocity dispersion σ_v is thus another element of the parameter vector $\boldsymbol{\theta}$.

However, we shall not a priori exclude the possibility of systematic velocity patterns in the cluster such as rotation and (non-isotropic) dilation. To a first approximation such patterns may be described as a linear velocity field, represented by the tensor $\boldsymbol{T}$ introduced in Appendix A of Paper I. The expected space velocity of a star at position $\boldsymbol{b}_i$ is then

$$\boldsymbol{u}_i \equiv \mathrm{E}(\boldsymbol{v}_i) = \boldsymbol{v}_0 + \boldsymbol{T}(\boldsymbol{b}_i - \boldsymbol{b}_0)\,, \tag{3}$$

where $\boldsymbol{b}_0$ is the centroid position.[1] In equatorial coordinates the components of $\boldsymbol{T}$ are the nine partial derivatives $T_{\alpha\beta} = \partial u_\alpha/\partial b_\beta$ for $\alpha, \beta = x, y, z$. However, as was shown in Paper I (Appendix A), only eight independent components of $\boldsymbol{T}$ can in principle be determined by the present method. The ninth component $\kappa \equiv \frac{1}{3}(T_{xx} + T_{yy} + T_{zz})$, representing an isotropic expansion or contraction of the cluster, cannot be separated from a change in $\boldsymbol{v}_0$ based on only astrometric data. To avoid a singularity in the ML equations it is therefore necessary to apply the constraint $\kappa = 0$ on the form of $\boldsymbol{T}$, or more generally to assume a fixed value for κ (e.g. the inverse age for an expanding association). Some other linear combinations of the tensor components have a simple physical interpretation. In particular, the anti-symmetric part of the tensor represents a rigid-body rotation about the centroid. We therefore use the following eight linearly independent components of $\boldsymbol{T}$ to represent the internal systematic velocity field:

$$\begin{aligned} \omega_x &= \tfrac{1}{2}(T_{zy} - T_{yz})\,, & w_1 &= \tfrac{1}{2}(T_{zy} + T_{yz})\,, \\ \omega_y &= \tfrac{1}{2}(T_{xz} - T_{zx})\,, & w_2 &= \tfrac{1}{2}(T_{xz} + T_{zx})\,, \\ \omega_z &= \tfrac{1}{2}(T_{yx} - T_{xy})\,, & w_3 &= \tfrac{1}{2}(T_{yx} + T_{xy})\,, \\ & & w_4 &= T_{xx}\,, \\ & & w_5 &= T_{yy}\,. \end{aligned} \tag{4}$$

[1] Actually $\boldsymbol{b}_0$ is an arbitrary reference position, namely the point in which the local velocity $\boldsymbol{u}(\boldsymbol{b})$ assumes the status of 'centroid' velocity $\boldsymbol{v}_0$. The coordinates of $\boldsymbol{b}_0$ can therefore be fixed in advance.

The components of $\boldsymbol{T}$ are uniquely determined by Eq. (4) and the assumed expansion rate κ, since $T_{zz} = 3\kappa - w_4 - w_5$. $\boldsymbol{\omega} = (\omega_x, \omega_y, \omega_z)$ is the angular velocity of the cluster, while $\boldsymbol{w} = (w_1, w_2, w_3, w_4, w_5)$ represents (non-isotropic) dilation. The components of $\boldsymbol{\omega}$ and $\boldsymbol{w}$ are additional elements of the general parameter vector $\boldsymbol{\theta}$.

The complete parameter vector is, therefore, $\boldsymbol{\theta} = (\boldsymbol{\pi}, \boldsymbol{v}_0, \sigma_v, \boldsymbol{\omega}, \boldsymbol{w})$. The total number of parameters is $m = n + 12$. Although this is our most general cluster model, we shall normally assume that the internal systematic velocities are negligible, in which case only the $m = n + 4$ parameters in $\boldsymbol{\theta} = (\boldsymbol{\pi}, \boldsymbol{v}_0, \sigma_v)$ are estimated. We refer to this restricted parameter set as the *basic cluster model*.

In summary, the pdf for the space velocity of star i is assumed to be Gaussian with mean value $\boldsymbol{u}_i$ [Eq. (3)] and covariance $\boldsymbol{S}$ [Eq. (2)]. The explicit form of the pdf is

$$p_v(\boldsymbol{v}_i \,|\, \boldsymbol{\theta}) \;=\; (2\Pi)^{-3/2} |\boldsymbol{S}|^{-1/2} \times \exp\left[-\tfrac{1}{2}(\boldsymbol{v}_i - \boldsymbol{u}_i)' \boldsymbol{S}^{-1} (\boldsymbol{v}_i - \boldsymbol{u}_i)\right] , \qquad (5)$$

where $\Pi = 3.14\ldots$ is the mathematical constant.

3.4. Observation model

For each star the observables are the trigonometric parallax (π_i) and the proper motion components in right ascension[2] ($\mu_{\alpha*i} \equiv \dot{\alpha}_i \cos\delta_i$) and declination ($\mu_{\delta i} \equiv \dot{\delta}_i$). These are collected in arrays

$$\boldsymbol{a}_i = \begin{bmatrix} \pi_i \\ \mu_{\alpha*i} \\ \mu_{\delta i} \end{bmatrix} \quad (i = 1 \ldots n) . \qquad (6)$$

The actually observed values are in the arrays $\widetilde{\boldsymbol{a}}_i$. It is assumed that the observations are unbiased,

$$\mathrm{E}(\widetilde{\boldsymbol{a}}_i - \overline{\boldsymbol{a}}_i) = \boldsymbol{0} , \qquad (7)$$

with known covariance matrices

$$\boldsymbol{C}_i = \mathrm{Cov}(\widetilde{\boldsymbol{a}}_i) \equiv \mathrm{E}\left[(\widetilde{\boldsymbol{a}}_i - \overline{\boldsymbol{a}}_i)(\widetilde{\boldsymbol{a}}_i - \overline{\boldsymbol{a}}_i)'\right] . \qquad (8)$$

The observational errors for the different stars, on the other hand, are assumed to be uncorrelated:

$$\mathrm{E}\left[(\widetilde{\boldsymbol{a}}_i - \overline{\boldsymbol{a}}_i)(\widetilde{\boldsymbol{a}}_j - \overline{\boldsymbol{a}}_j)'\right] = \boldsymbol{0} \quad (i \neq j) . \qquad (9)$$

[This assumption does not hold strictly e.g. for Hipparcos data. We discuss this further in Sect. 5.4.] Gaussian error distributions are assumed. The pdf for the observables, conditional upon their true values, is then

$$p_a(\widetilde{\boldsymbol{a}}_i \,|\, \overline{\boldsymbol{a}}_i) \;=\; (2\Pi)^{-3/2} |\boldsymbol{C}_i|^{-1/2} \times \exp\left[-\tfrac{1}{2}(\widetilde{\boldsymbol{a}}_i - \overline{\boldsymbol{a}}_i)' \boldsymbol{C}_i^{-1} (\widetilde{\boldsymbol{a}}_i - \overline{\boldsymbol{a}}_i)\right] . \qquad (10)$$

Astrometry also provides the barycentric right ascension (α_i) and declination (δ_i) of each star for a certain epoch. For the present purpose the positional data can be regarded as error-free and defining the unit vector $\boldsymbol{r}_i$ from the solar system barycentre towards the star. Two more auxiliary unit vectors, tangent to the unit sphere at $\boldsymbol{r}_i$, are needed: $\boldsymbol{p}_i$ in the direction of increasing right ascension (local 'East'), and $\boldsymbol{q}_i$ in the direction of increasing declination (local 'North'). $\boldsymbol{p}_i$, $\boldsymbol{q}_i$ and $\boldsymbol{r}_i$ form a right-handed orthogonal coordinate frame known as the 'normal triad' at $\boldsymbol{r}_i$ with respect to the equatorial frame (Murray 1983). The explicit formulae for these vectors are given in Eq. (A.2).

Given the position $\boldsymbol{b}_i$ and velocity $\boldsymbol{v}_i$ of a star, the 'true' observables are calculated as

$$\overline{\boldsymbol{a}}_i = \begin{bmatrix} \pi_i \\ \boldsymbol{p}_i' \boldsymbol{v}_i \pi_i / A \\ \boldsymbol{q}_i' \boldsymbol{v}_i \pi_i / A \end{bmatrix} \qquad (11)$$

where $A \simeq 4.74047$ km yr s^{-1} is the astronomical unit. If there were no velocity dispersion ($\sigma_v = 0$), then $\boldsymbol{u}_i$ from Eq. (3) could be substituted for $\boldsymbol{v}_i$ in Eq. (11) and the pdf for the observables in Eq. (14) could immediately be written conditional upon the model parameters π_i and $\boldsymbol{v}_0$, as required for the ML estimation.

In the presence of a non-zero velocity dispersion, however, $\boldsymbol{v}_i$ is itself a random variable with pdf according to Eq. (5). The joint pdf of the observables with the velocity is

$$p_{av}(\widetilde{\boldsymbol{a}}_i, \boldsymbol{v}_i \,|\, \pi_i) = p_a[\widetilde{\boldsymbol{a}}_i \,|\, \overline{\boldsymbol{a}}_i(\boldsymbol{v}_i, \pi_i)] p_v(\boldsymbol{v}_i \,|\, \boldsymbol{\theta}) , \qquad (12)$$

since the observational errors are assumed to be independent of the random velocities. The pdf of the observables is then obtained as the marginal density

$$p(\widetilde{\boldsymbol{a}}_i \,|\, \boldsymbol{\theta}) = \iiint_{-\infty}^{+\infty} p_{av}(\widetilde{\boldsymbol{a}}_i, \boldsymbol{v}_i \,|\, \pi_i) \, \mathrm{d}^3\boldsymbol{v}_i . \qquad (13)$$

This integral can be evaluated analytically after insertion of p_v and p_a from Eqs. (5) and (10) in Eq. (12). Since the product of two normal probability density functions is normal, and the marginal density of a normal pdf is also normal, it follows that p is normal and can be written

$$p(\widetilde{\boldsymbol{a}}_i \,|\, \boldsymbol{\theta}) \;=\; (2\Pi)^{-3/2} |\boldsymbol{D}_i|^{-1/2} \times \exp\left[-\tfrac{1}{2}(\widetilde{\boldsymbol{a}}_i - \boldsymbol{c}_i)' \boldsymbol{D}_i^{-1} (\widetilde{\boldsymbol{a}}_i - \boldsymbol{c}_i)\right] . \qquad (14)$$

We find that

$$\boldsymbol{c}_i = \begin{bmatrix} \pi_i \\ \boldsymbol{p}_i' \boldsymbol{u}_i \pi_i / A \\ \boldsymbol{q}_i' \boldsymbol{u}_i \pi_i / A \end{bmatrix} \qquad (15)$$

and, using the isotropic dispersion tensor from Eq. (2),

$$\begin{aligned} \boldsymbol{D}_i \;&=\; \boldsymbol{C}_i + \begin{bmatrix} 0 & 0 & 0 \\ 0 & \boldsymbol{p}_i' \boldsymbol{S} \boldsymbol{p}_i & \boldsymbol{p}_i' \boldsymbol{S} \boldsymbol{q}_i \\ 0 & \boldsymbol{q}_i' \boldsymbol{S} \boldsymbol{p}_i & \boldsymbol{q}_i' \boldsymbol{S} \boldsymbol{q}_i \end{bmatrix} (\pi_i / A)^2 \\ &=\; \boldsymbol{C}_i + \begin{bmatrix} 0 & 0 & 0 \\ 0 & \sigma_v^2 & 0 \\ 0 & 0 & \sigma_v^2 \end{bmatrix} (\pi_i / A)^2 . \end{aligned} \qquad (16)$$

[2] Following the convention established in the Hipparcos and Tycho Catalogues (ESA 1997) quantities measured as true arcs on the sky are indicated by an asterisk, as in $\mu_{\alpha*} \equiv \mu_\alpha \cos\delta$.

3.5. The likelihood function

Since the observational errors and random velocities of the individual stars are assumed to be statistically independent, the pdf of the whole set of observables equals the product of the individual pdf's. The log-likelihood function is, therefore,

$$\begin{aligned}\mathcal{L}(\boldsymbol{\theta}) &= \ln \prod_{i=1}^{n} p(\widetilde{\boldsymbol{a}}_i \,|\, \boldsymbol{\theta}) \\ &= -\frac{3n}{2}\ln(2\Pi) - \frac{1}{2}\sum_{i=1}^{n}\ln|\boldsymbol{D}_i| \\ &\quad -\frac{1}{2}\sum_{i=1}^{n}(\widetilde{\boldsymbol{a}}_i-\boldsymbol{c}_i)'\boldsymbol{D}_i^{-1}(\widetilde{\boldsymbol{a}}_i-\boldsymbol{c}_i)\,, \end{aligned} \tag{17}$$

where $\boldsymbol{c}_i$ and $\boldsymbol{D}_i$ depend on $\boldsymbol{\theta}$ through Eq. (15) and (16). The ML estimate $\widehat{\boldsymbol{\theta}}$ is obtained by finding the maximum of $\mathcal{L}(\boldsymbol{\theta})$, or, equivalently, the minimum of

$$U(\boldsymbol{\theta}) = \sum_{i=1}^{n}\ln|\boldsymbol{D}_i| + \sum_{i=1}^{n} g_i(\boldsymbol{\theta})\,, \tag{18}$$

where

$$g_i(\boldsymbol{\theta}) = (\widetilde{\boldsymbol{a}}_i-\boldsymbol{c}_i)'\boldsymbol{D}_i^{-1}(\widetilde{\boldsymbol{a}}_i-\boldsymbol{c}_i)\,. \tag{19}$$

The practical algorithm to find the maximum of $\mathcal{L}(\boldsymbol{\theta})$ is discussed in Appendix A.

3.6. Radial-velocity estimates

Given the set of estimated parameters $\widehat{\boldsymbol{\theta}}$ the astrometric radial velocity of star i is computed as the line-of-sight projection of the estimated (non-random) stellar space velocity in Eq. (3). For the basic cluster model (with $\boldsymbol{T}=\boldsymbol{0}$) this reduces to

$$\widehat{v}_{ri} = \boldsymbol{r}_i'\widehat{\boldsymbol{v}}_0\,. \tag{20}$$

It should be noted that the error in this quantity is the sum of two statistically independent components: (1) the radial component of the estimation error in $\widehat{\boldsymbol{v}}_0$, and (2) the radial component of the peculiar velocity of the star, $\boldsymbol{v}_i-\boldsymbol{u}_i$; see Eq. (A.18).

3.7. Rejection of outliers

Our formulation of the cluster model does not take into account that the observational material may include field stars which do not share the common (mean) space velocity of the cluster. The ML method requires that the model provide a statistically correct description of the data. In particular, it must only be applied to the actual members of the cluster, or rather to members whose mean space motion during the observing period agrees with the model. In practice this rules out also a number of close binaries, even if they are members of the cluster, since the short-term motions of their photocentres may deviate significantly from the motion of their centres of mass. Because of the high frequency of duplicity and the wide distribution of separations and periods, the subset of astrometrically detectable binaries blends continuously with the non-perturbed, single member stars. The elimination of outliers, whether members or not, is therefore an equally important and delicate part of the application of the moving-cluster method.

Outliers can be detected by computing a suitable goodness-of-fit statistic for each star in the solution. The quantity $g_i \equiv g_i(\widehat{\boldsymbol{\theta}})$, where $g_i(\boldsymbol{\theta})$ is defined by Eq. (19), is a quadratic measure of the distance between the observed and fitted vector $\boldsymbol{a}_i$, weighted by the inverse of the expected covariance of the difference. Therefore, g_i can be used for detection of outliers. In order to define a suitable rejection criterion it is desirable to know, at least approximately, the distribution of g_i in the nominal case when the data behave according to the model.

The quadratic form in Eq. (19) and the assumption of Gaussian errors suggest that g_i should approximately follow a chi-square distribution. There are $3n$ observables and $n+4$ parameters in the basic cluster model, and consequently $2n-4$ degrees of freedom, or $\simeq 2$ degrees of freedom for each g_i (if n is not small). In simulations using Gaussian distributions for the peculiar velocities and observation errors we find that a *scaled* version of g_i is very nearly distributed as χ^2_2. That is,

$$\Pr(g_i > g) \simeq \exp(-\beta g/2) \tag{21}$$

where β is a scaling factor to be determined by the simulations (Sect. 3.8). For a given level of significance α the star should therefore be rejected if $g_i > g_{\rm lim}$, where

$$g_{\rm lim} = -2(\ln\alpha)/\beta\,. \tag{22}$$

In simulations of Hyades data (Sect. 4.1.3) we find $\beta \simeq 0.66$, so that a 1 per cent significance level requires $g_{\rm lim} \simeq 14$. As discussed in Sect. 4.2, it is possible to derive an optimal value for $g_{\rm lim}$ if the distribution of peculiar velocities can be properly modelled.

A complication with this rejection procedure is that the goodness-of-fit statistics g_i depend on the estimated σ_v through Eq. (16). Eliminating outliers will however decrease the estimated velocity dispersion and consequently increase the g_i values. This, in turn, will in general cause other stars to fall beyond the adopted acceptance limit. It is not obvious how to find the maximum subset of stars for which all $g_i \le g_{\rm lim}$, or if this subset is unique or even exists. Testing each of the $\simeq 2^n$ possible subsets is obviously not a viable method for $n \gtrsim 20$.

As a practical (if not necessarily optimal) solution we have adopted a sequential rejection procedure, in which the one star with the largest g_i ($= g_{\rm max}$) is removed from the sample. A new solution is then computed, including new g_i values. The process is repeated, removing the star with the largest g_i and computing a new solution, until all $g_i \le g_{\rm lim}$. In some cases it may happen that the solution becomes unstable before this criterion is satisfied. In those cases where this happens when $\widehat{\sigma}_v$ has been reduced to practically zero, the number of model parameters could be reduced, e.g. by assuming $\sigma_v = 0$.

3.8. Use of numerical simulations

Monte Carlo simulation of the ML estimation problem is essential for studying the efficiency and convergence of the adopted procedure, as well as the precision and possible bias of the resulting estimates. In a Monte Carlo simulation, a set of 'true' parameters $\overline{\boldsymbol{\theta}}$ is assumed and from this, many realisations of hypothetical ('observed') data $\widetilde{\boldsymbol{a}}$ are generated according to the adopted model. Random observational errors and other variations, in our case due to the internal velocity dispersion, are simulated by means of a random number generator. Applying the estimation algorithm to each hypothetical data set results in an estimated parameter vector $\widehat{\boldsymbol{\theta}}$. From the assembly of these vectors one can determine various statistics, in particular the bias $B = \langle\widehat{\theta} - \overline{\theta}\rangle$ and rms scatter $S = \langle(\widehat{\theta} - \langle\widehat{\theta}\rangle)^2\rangle^{1/2}$ of the individual parameter θ.

Synthetic cluster data are generated according to the following general recipe. First, the overall characteristics of the cluster and observations are specified: the number of stars n and their positions $\boldsymbol{b}_i$ relative to the Sun, the centroid velocity $\boldsymbol{v}_0$, descriptions of systematic and random internal motions, and the observational accuracies. These data define the 'true' parameter vector $\overline{\boldsymbol{\theta}}$ as well as the (error-free) auxiliary quantities $\boldsymbol{r}_i$ and $\boldsymbol{C}_i$. Next, the true velocities of the individual stars are computed as $\boldsymbol{v}_i = \boldsymbol{v}_0 + \boldsymbol{T}(\boldsymbol{b}_i - \boldsymbol{b}_0) + \boldsymbol{\eta}_i$, where $\boldsymbol{T}$ follows from Eq. (4) and the Cartesian components of $\boldsymbol{\eta}_i$ are drawn from independent Gaussian distributions with mean value zero and standard deviation σ_v. The true observables are then computed from Eq. (11). Finally, observation noise with covariance $\boldsymbol{C}_i$ is added to give the hypothetical data set $\widetilde{\boldsymbol{a}}_i$.[3]

We use the following terminology: an *experiment* is a single realisation of 'observed' data, plus the subsequent estimation of model parameters. A *simulation* is the assembly of N such experiments based on a fixed set of model parameters and auxiliary data, but with different realisations of the random variables. An important question is how big N needs to be. The precision by which the bias can be estimated is $\simeq S/\sqrt{N}$, where S is the rms scatter of the estimated values. To ascertain the level of biases, and compute the corresponding corrections, it is usually sufficient to know them to within 10 per cent of the scatter, which requires $N \gtrsim 100$. However, one additional purpose of the simulations is to check the formal standard errors based on the Cramér–Rao bound, Eq. (1). A relative precision of the order of 1 per cent in the scatter is then desirable. For a normal distribution the relative precision of the scatter (sample standard deviation) is $\simeq 1/\sqrt{2N}$. To reach a precision of 1 per cent, the simulations should consequently consist of $N \gtrsim 5000$ experiments each.

[3] The general procedure to generate a k-dimensional vector $\boldsymbol{x}$ of centred observation errors with given covariance matrix $\boldsymbol{C}$ ($k \times k$) is as follows: use the Cholesky factorisation algorithm (Press et al. 1992) to compute the lower-triangular matrix $\boldsymbol{L}$ such that $\boldsymbol{L}\boldsymbol{L}' = \boldsymbol{C}$. Then generate a vector $\boldsymbol{\nu}$ of k independent unit normal deviates and compute $\boldsymbol{x} = \boldsymbol{L}\boldsymbol{\nu}$. Since $\mathrm{E}(\boldsymbol{\nu}) = \boldsymbol{0}$ and $\mathrm{E}(\boldsymbol{\nu}\boldsymbol{\nu}') = \boldsymbol{I}$, it follows that $\mathrm{E}(\boldsymbol{x}) = \boldsymbol{0}$ and $\mathrm{E}(\boldsymbol{x}\boldsymbol{x}') = \boldsymbol{C}$, as required.

4. Monte Carlo simulations of a test case

To investigate properties of the ML estimator we use the Hyades cluster as a test case. Based on kinematic criteria, including spectroscopic radial velocities, Perryman et al. (1998) identified 197 stars from the Hipparcos Catalogue as probable members of the Hyades (stars with '1' in column x of their Table 2). This sample is subsequently referred to as 'Hy0'. The positions and distances of these stars, as determined by Hipparcos, define the three-dimensional structure of the cluster assumed in all our simulations. The astrometric accuracies ($\boldsymbol{C}_i$) are also taken directly from the Hipparcos Catalogue. In equatorial coordinates the centroid velocity of the cluster is taken to be $\overline{\boldsymbol{v}}_0 = (-6.32, +45.24, +5.30)$ km s^{-1}, as found by Perryman et al. (1998) for the inner 20 pc of the cluster, and from the same authors we take the centroid position to be $\boldsymbol{b}_0 = (+17.7, +41.2, +13.3)$ pc.

4.1. Solutions based on consistent cluster models

In this section we examine the performance of the ML estimator in the case when the model assumed in the solution correctly describes the actual kinematics of the cluster. The purpose is to determine the possible biases that are intrinsic to the method, and its behaviour under ideal circumstances. In Sect. 4.2, we then consider how deviations from the assumed model will affect the results.

4.1.1. Precision and bias of estimates

Results from 5000 experiments with the basic cluster model applied to the 197 stars in sample Hy0 are summarised in Table 1 (simulation **a**). A value of 0.30 km s^{-1} was taken for the true velocity dispersion (Perryman et al. 1998). It is seen that, as a mean of the many experiments, the parallaxes are within ± 0.01 mas of their true values, and the estimated centroid velocity vector within ± 0.01 km s^{-1} of the true vector. As a consequence, the bias in the radial component of the centroid velocity is only 0.01 km s^{-1}. However, the velocity dispersion is significantly underestimated (0.15 versus the true value 0.30 km s^{-1}).

In simulation **a**, all the model parameters are thus recovered without any significant bias, except σ_v, which is severely underestimated. On the other hand, the uncertainties of *all* the estimated parameters are significantly underestimated (roughly by 25 per cent, i.e. $\epsilon(\widehat{\theta}) \simeq 0.75S$). This latter circumstance is probably a consequence of the underestimated σ_v, which through Eq. (16) gives a too low value for the total variance of the observables. Even if we are (here) not primarily interested in estimating the velocity dispersion per se, it is thus important to understand why it is so strongly underestimated in the solutions. This problem is further investigated in Sect. 4.3.

The simulations described above all used the basic cluster model, in which no systematic velocity field is included. In simulation **b** of Table 1 we added a pure rotation ($\boldsymbol{\omega}$), and in **c** a rotation plus the remaining terms ($\boldsymbol{w}$) due to non-isotropic dilation. In both cases the ML estimation was made with exactly the

Table 1. Results of Monte Carlo simulations for the Hyades sample Hy0 with $n = 197$ stars. Each simulation (**a** to **c**) comprises 5000 experiments and the results are described by the following quantities: $\overline{\theta}$ = assumed ('true') parameter value; $\langle\widehat{\theta}\rangle$ = mean estimated parameter value; $\langle\epsilon(\widehat{\theta})\rangle$ = mean estimated standard error of the parameter; $S = \langle(\widehat{\theta} - \langle\widehat{\theta}\rangle)^2\rangle^{1/2}$ = rms scatter of the estimates. The columns correspond to the model parameters π_i and v_{0x} through w_5 and, in the final column, the radial component of the centroid velocity (v_{0r}). For the parallaxes, the statistics refer to the deviations from the true values ($\pi_i - \overline{\pi}_i$).

$\theta =$	$\pi_i - \overline{\pi}_i$	v_{0x}	v_{0y}	v_{0z}	σ_v	ω_x	ω_y	ω_z	w_1	w_2	w_3	w_4	w_5	v_{0r}
	[mas]	.....	[km s^{-1}]	.....		.....			[km s^{-1} kpc^{-1}]		.....			[km s^{-1}]
a Basic cluster model:														
$\overline{\theta}$	0.00	−6.32	+45.24	+5.30	0.30									+38.97
$\langle\widehat{\theta}\rangle$	−0.00	−6.32	+45.25	+5.30	0.15									+38.98
$\langle\epsilon(\widehat{\theta})\rangle$	0.32	0.09	0.25	0.07	0.02									0.26
S	0.43	0.12	0.31	0.09	0.03									0.33
b Cluster model including rotation:														
$\overline{\theta}$	0.00	−6.32	+45.24	+5.30	0.30	+20.0	+20.0	+20.0						+38.97
$\langle\widehat{\theta}\rangle$	−0.02	−6.27	+45.40	+5.34	0.15	+14.6	+20.9	+31.1						+39.14
$\langle\epsilon(\widehat{\theta})\rangle$	0.33	0.09	0.26	0.07	0.02	2.8	3.7	5.4						0.27
S	0.47	0.13	0.33	0.10	0.03	3.8	5.0	7.0						0.35
c Cluster model including rotation and non-isotropic dilation:														
$\overline{\theta}$	0.00	−6.32	+45.24	+5.30	0.30	+20.0	+20.0	+20.0	+20.0	+20.0	+20.0	+20.0	+20.0	+38.97
$\langle\widehat{\theta}\rangle$	−0.05	−6.37	+45.33	+5.30	0.15	+9.0	+17.0	+48.8	+29.9	+19.0	+40.1	+3.0	+38.1	+39.02
$\langle\epsilon(\widehat{\theta})\rangle$	0.35	0.16	0.37	0.12	0.02	24.3	6.6	20.2	22.7	6.4	21.6	9.0	16.0	0.41
S	0.57	0.20	0.46	0.15	0.03	24.4	8.1	21.3	22.8	8.2	23.6	11.4	17.5	0.51

same model as was used to generate the data, i.e. with a total of $n+7$ model parameters in **b** and $n+12$ in **c**. No expansion rate ($\kappa = 0$) was assumed. The non-zero components of $\boldsymbol{\omega}$ and $\boldsymbol{w}$ were all arbitrarily set to $+20$ km s^{-1} kpc^{-1}. It is seen that the assumed systematic velocity terms are approximately recovered in the solutions, albeit with biases that are of the same order as the formal uncertainties $\epsilon(\widehat{\theta})$. An important observation is that the centroid radial velocity (v_{0r}) remains practically unbiased, even if the velocity field terms are not. The inclusion of more parameters in the solution naturally increases both the formal uncertainties and the actual scatter of the estimates. We conclude that a linear velocity field (without general expansion), if it exists, can be determined with the present method. The resulting astrometric radial velocities are unbiased, but the statistical uncertainties are larger than for the basic cluster model. If we include an isotropic expansion in the simulation of data, the estimated centroid radial velocity is biased according to Eq. (10) in Paper I. The other basic model parameters remain unbiased.

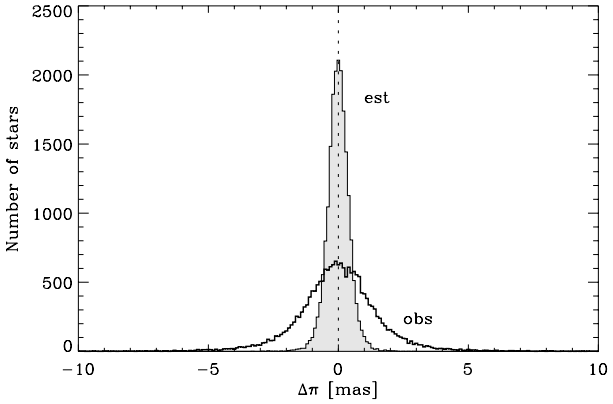

Fig. 2. Distribution of parallax errors in simulation **a** (Table 1): the histogram labelled 'obs' is for the observational errors ($\widehat{\pi}_i - \overline{\pi}_i$, standard deviation 1.76 mas), while 'est' is for the estimation errors ($\widehat{\pi}_i - \overline{\pi}_i$, standard deviation 0.43 mas).

4.1.2. Kinematically improved parallaxes

Fig. 2 shows the distribution of parallax errors in simulation **a**. The estimation errors in the parallaxes are significantly smaller than the observational errors assumed in the input data for the solutions. As discussed in Sect. 6.3 of Paper I this can be understood as resulting from a combination of the original trigonometric parallaxes with the kinematic parallaxes derived from the observed proper motions and the fitted kinematic parameters. We call these 'kinematically improved parallaxes', as they are neither trigonometric, nor (purely) kinematic. The kinematically improved parallaxes, here seen as a by-product of the determination of astrometric radial velocities, are by themselves highly interesting e.g. for a better definition of the Hertzsprung–Russell diagram for several clusters and associations (Dravins et al. 1997; Madsen 1999; de Bruijne 1999).

The rms error of 0.43 mas for the kinematically improved parallaxes indicated in Fig. 2 is in reasonable agreement with the theoretical Eq. (11) of Paper I. Assuming $\epsilon(\pi_{\rm trig}) = 1.76$ mas, $\epsilon(\mu) = 1.6\,\mathrm{mas\,yr^{-1}}$ (representative for $\mu_{\alpha*}$), $\sigma_v = 0.3\,\mathrm{km\,s^{-1}}$, and other data as in Table 4 of Paper I, the latter equation gives $\epsilon(\widehat{\pi}) \simeq 0.39$ mas.

The standard deviation of the normalised estimation error $(\widehat{\pi}_i - \overline{\pi}_i)/\epsilon(\widehat{\pi}_i)$ is 1.28. The formal errors of the estimated parallaxes thus need to be increased by 28 per cent to be consistent with the scatter found in the Monte Carlo experiments.

4.1.3. Distribution of the goodness-of-fit values

Fig. 3 shows the cumulative distribution of the g_i values from simulation **a** in Table 1 (solid curve). For comparison, the thick gray line shows the χ^2_2 distribution (with slope -0.5 in the lin-log diagram) expected on theoretical grounds as explained in Sect. 3.7. The empirical distribution is indeed very nearly exponential, but with a slope of $\simeq -0.33$. The scaling factor in Eq. (21) is, therefore, $\beta \simeq 0.66$ in this simulation. This is in rough quantitative agreement with the previous conclusion that the total covariances $\boldsymbol{D}_i$ are too small as a consequence of the underestimation of σ_v.

The distribution of the g_i values is of course modified by the rejection procedure described in Sect. 3.7, whereby an upper limit $g_{\max}$ is introduced. As shown by the dashed curves in Fig. 3, this procedure produces a gently truncated exponential distribution of the g_i values, without much affecting the distribution of the small values.

4.2. Robustness

Robustness refers to the desirable property of an estimator that the results are relatively insensitive to deviations from the model assumptions. In the context of the basic cluster model two types of deviation have been considered: systematic velocity patterns, and deviations from a Gaussian velocity distribution. The latter may be caused either by individual contaminating field stars or astrometric binaries, or by a more general shape of velocity distribution (e.g. a mixture of different dispersions).

The existence of systematic velocity patterns can at least partly be dealt with by solving components of a linear velocity field as discussed in Sect. 3.3. However, in practice this solution would not be accepted unless it gave a significant result for the linear velocity terms. We should therefore consider the possible biases in the basic solution produced by velocity fields that are weak enough to remain undetected. Given the formal errors and scatters in simulations **b** and **c** (Table 1), it is clear that components in $\boldsymbol{\omega}$ and $\boldsymbol{w}$ (or equivalently in $\boldsymbol{T}$) of the order of 10 km s^{-1} kpc^{-1} would generally remain undetected. Simulations were made, in which the components of $\boldsymbol{\omega}$ and $\boldsymbol{w}$ were randomly assigned values with a uniform distribution in the interval ± 10 km s^{-1} kpc^{-1}. In each experiment the centroid velocity was estimated by means of the basic cluster model, i.e. without solving for the linear velocity field. The resulting rms scatter in the astrometric radial velocity of the cluster centroid was 0.43 km s^{-1}. This should be compared with the scatter of 0.34 km s^{-1} obtained in simulation **a** without linear velocity fields, but with otherwise identical assumptions. The increased scatter (by 0.26 km s^{-1} in quadrature) is in very good agreement with the theoretically expected 0.27 km s^{-1} derived from Eq. (A6) in Paper I.

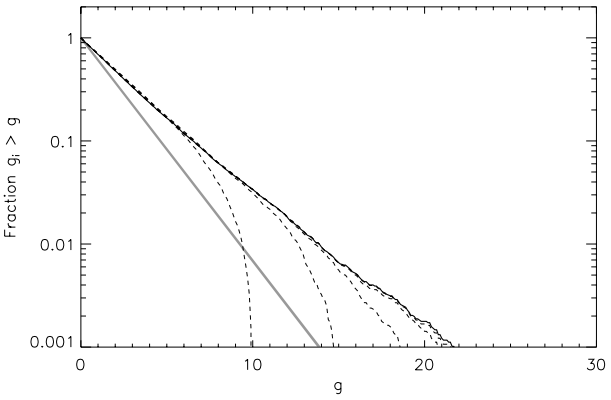

Fig. 3. Cumulative distribution of the goodness-of-fit values g_i obtained in simulation **a** of Table 1 (solid curve) and with cut-off values $g_{\lim} = 30$, 25, 20, 15, and 10 (dashed curves). The thick gray line is for a chi-square distribution with 2 degrees of freedom. In these simulations, the internal velocities follow a Gaussian distribution with dispersion $\sigma_v = 0.3$ km s^{-1}.

The use of (primarily) kinematic criteria to identify probable cluster members, e.g. for the Hyades by Perryman et al. (1998), precludes that the input sample for the ML estimation contains a large number of field stars. Also member stars with strongly deviating proper motion (due to binarity) are rejected a priori. However, a small number of stars could still have peculiar velocities exceeding several times the combined standard deviation of observational errors and σ_v. The rejection procedure described in Sect. 3.7 is intended to eliminate such outliers. To test the effectiveness of the procedure, we made a simulation in which the peculiar velocity of an individual star, with probability 0.05, was multiplied by a factor 10. The centroid astrometric accuracy was estimated with different rejection limits $g_{\lim}$. The rms scatter was 0.56 km s^{-1} for the full sample ($g_{\lim} = \infty$) and reached a shallow minimum of 0.35 km s^{-1} for $g_{\lim} \simeq 15$, with a mean rejection rate about 0.05. Since this minimum is very close to what is obtained for the full, uncontaminated sample, we conclude that the rejection procedure is very efficient for this type of outliers.

In reality we do not expect such a clear-cut distinction between well-behaved member stars and outliers. A more likely situation is that of a continuous blend of populations with different kinematic characteristics. A simple model for this is to assume that the velocity dispersion σ_v itself is a random variable. Since the dispersion must be positive, a convenient assumption is that it follows a log-normal distribution with median value $\sigma_{v,\mathrm{med}}$ and logarithmic standard width γ (thus $\ln \sigma_v$ is Gaussian with mean value $\ln \sigma_{v,\mathrm{med}}$ and standard deviation γ). With $\sigma_{v,\mathrm{med}} = 0.3$ km s^{-1} and $\gamma = 1$ we found that the scatter in the centroid radial velocity was 0.44, 0.42, 0.40, 0.38, 0.40 km s^{-1} for $g_{\lim} = \infty$, 25, 20, 15 and 10, respectively. A cut-off limit around 15 thus appears optimal also in this case. The non-Gaussian nature of the internal velocities is clearly revealed in the statistics of the residuals, as shown by the distribution of g_i values in Fig. 4. This may be a useful diagnostic for the study of real cluster data (Sect. 5).

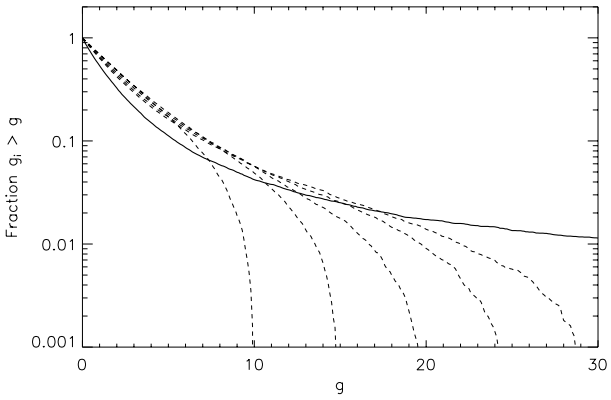

Fig. 4. Cumulative distribution of the goodness-of-fit values g_i obtained in simulations with a non-Gaussian velocity distribution. As in Fig. 3, the different curves are for different cut-off values $g_{\rm lim} = \infty$ (solid curve) and 30, 25, 20, 15, 10 (dashed curves). In these experiments, σ_v was modelled as a log-normal random variable with median 0.3 km s^{-1} and standard deviation 1.0 in $\ln \sigma_v$.

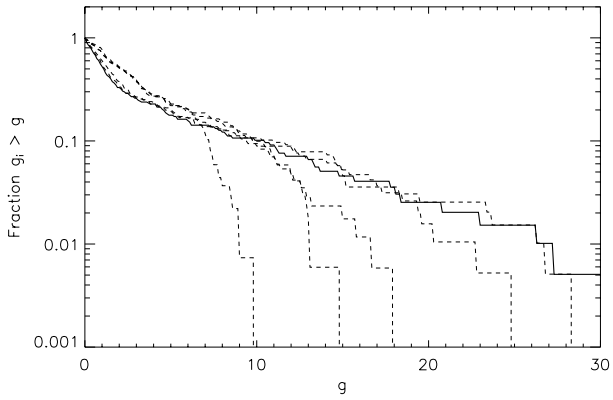

Fig. 5. Cumulative distribution of the goodness-of-fit values g_i for the actual Hipparcos data for Hyades sample Hy0. The different curves are for different cut-off values $g_{\rm lim} = \infty$ (solid lines), and 30, 25, 20, 15, 10 (dashed lines). This diagram should be compared with the theoretical distributions obtained in simulations, viz. Fig. 3 for a purely Gaussian internal velocity distribution and Fig. 4 for one example of a non-Gaussian distribution. The real Hyades data contain strong evidence for a deviation from Gaussian velocities.

A rejection procedure using $g_{\rm lim} = 15$ thus appears to provide excellent protection against outliers and works very well also in more general cases of non-Gaussian velocity dispersions. The accuracy of the resulting centroid velocity is only marginally degraded compared with the nominal case of a Gaussian velocity dispersion.

4.3. Unbiased estimation of the velocity dispersion

It was noted in Sect. 4.1.1 that the internal velocity dispersion σ_v is strongly underestimated in the ML solutions based on simulated observations. We now turn to investigating this effect more closely, and to finding a remedy for it.

The bias in the ML estimate of $\widehat{\sigma}_v$ apparent in Table 1 is probably related to the circumstance that we assume an isotropic three-dimensional dispersion of the peculiar velocities $\boldsymbol{\eta}_i$, while in practice only one component can be measured astrometrically, viz. $\eta_{\perp i}$ perpendicular to the plane containing the line of sight and the centroid velocity vector. The radial component η_{ri} of the peculiar velocities is obviously not determined at all, since that would require spectroscopic velocities. The remaining tangential component $\eta_{\parallel i}$, parallel to the plane containing the line of sight and the centroid velocity, is largely absorbed by the individual distance estimates (provided that $\epsilon(\mu)/\mu < \epsilon(\pi)/\pi$, as is the case for the Hyades cluster). Thus the measured variance in one direction ($\perp$) is effectively 'spread out' in all three directions, causing the estimated σ_v to come out much too small. The effect is compounded by the observational errors in the proper motions, which are implicitly taken into account in the ML estimation by reducing $\widehat{\sigma}_v$ even further. This explains, at least qualitatively, why we obtain $\widehat{\sigma}_v = 0$ in simulations where the true dispersion is less than a certain value ($\simeq 0.14$ km s^{-1} for the Hyades case).

It should be remarked here that the existence of this bias does not imply that the present formulation or implementation of the ML method would not be valid. While the ML method is known to perform well in many practical situations, there is no guarantee that it provides unbiased estimates. In the present case the bias seems to be the consequence of an intrinsic anisotropy of the astrometric observations with respect to the mathematical cluster model.

The referee has drawn our attention to a practical way in which this difficulty could be avoided, using a variant of the procedure described by Narayanan & Gould (1999a). Instead of forcing a solution with the – physically well motivated – isotropic dispersion, let us assume a triaxial velocity ellipsoid with dispersions $\sigma_\parallel$, $\sigma_\perp$, σ_r along the previously defined axes. Applying the ML estimation to this model will of course give much too small a value for $\sigma_\parallel$ and an undetermined σ_r. However, $\sigma_\perp$ may be obtained without bias, and that value could then be adopted as the actual dispersion in all three axes. (Narayanan & Gould use also spectroscopic radial velocities and photometric distances, and so are able to obtain information on all three components; they then impose an isotropic dispersion using the best combined estimate.)

We have not adopted that method, mainly because there is a mathematical inconsistency involved in forcing σ_r and $\sigma_\parallel$ to equal the independently estimated $\sigma_\perp$. However, along a similar line of thought we found another way to deal with the problem. From the proper-motion residuals of the ML solution we compute estimates of the peculiar velocity components $\eta_{\perp i}$ and of their observational uncertainties $\epsilon(\eta_{\perp i})$. A posteriori analysis of these data provides an estimate of $\sigma_\perp$, and hence of σ_v under the hypothesis of isotropic dispersion. Details of the procedure are given in Appendix A.4. Table 2 shows that $\widehat{\sigma}_\perp$ calculated in this way is a practically unbiased estimate of σ_v even for very small dispersions. This value can then be used in Monte Carlo simulations to derive the true uncertainties in all the estimated parameters.

Table 2. Results of Monte Carlo simulations corresponding to case **a** in Table 1 (the Hyades sample Hy0 with 197 stars), but for different values of the assumed velocity dispersion and including results from the analysis of proper motion residuals. $\overline{\sigma}_v$ = assumed ('true') velocity dispersion; $\widehat{\sigma}_v$ = velocity dispersion obtained by the standard ML estimation method of Sect. 3; $\widehat{\sigma}_\perp$ = velocity dispersion normal to the cluster motion, calculated according to Sect. 4.3 and Appendix A.4. The table gives mean values $\langle\,\rangle$ and rms scatter S from simulations with 200 experiments each. All values are in km s^{-1}.

$\overline{\sigma}_v$	$\langle\widehat{\sigma}_v\rangle\ \pm S$	$\langle\widehat{\sigma}_\perp\rangle\ \pm S$
0.0	0	0.023±0.033
0.1	0	0.092±0.032
0.2	0.039±0.038	0.197±0.028
0.3	0.153±0.029	0.297±0.028
0.4	0.241±0.026	0.398±0.031
0.5	0.324±0.028	0.497±0.035

5. Hyades: Results from Hipparcos data

In this section we briefly discuss the application of the procedures described in the previous sections to the actual Hipparcos observations of the Hyades cluster. As the purpose is not to make an in-depth study of the cluster kinematics, we restrict the application to the basic cluster model.

5.1. The formal maximum-likelihood solution

Starting from the sample Hy0 defined in Sect. 4, we made a succession of solutions for decreasing rejection threshold $g_{\rm lim}$. Results for the common cluster parameters $\boldsymbol{v}_0$ and σ_v, with formal error estimates, are given in the upper part of our Table 3. The corresponding estimates of the centroid radial velocity $v_{0r} = \boldsymbol{r}_0'\boldsymbol{v}_0$ (Eq. A.16) are also given. As expected, the estimated dispersion decreases with $g_{\rm lim}$, while the solution for $\boldsymbol{v}_0$ is relatively stable after the first few (worst) outliers have been removed. The formal errors also decrease in the sequence of solutions, but as discussed in Sect. 4 this does not necessarily reflect the true uncertainties.

The rapid decrease in $\widehat{\sigma}_v$ from $g_{\rm lim} = 25$ to 20 (with n decreasing from 191 to 171) suggests that most of the dispersion can be attributed to a relatively small fraction of the stars. To examine this further, we show in Fig. 5 the distribution of g_i values in the successive solutions. The distributions are rather different from the truncated exponentials expected for a Gaussian velocity dispersion (Fig. 3), but qualitatively similar to the ones in Fig. 4, for a continuous (log-normal) mix of dispersions.

Part of the large dispersion in the full Hy0 sample may be caused by double and multiple stars, in particular astrometric binaries with deviating proper motions for the centre of light. Many of the stars in the sample Hy0 are actually known visual or spectroscopic binaries, and several more were indicated in the Hipparcos Catalogue as possible astrometric binaries or suspected resolved systems. The most doubtful cases are those flagged in columns s or u in Table 3 of Perryman et al. (1998), and those visual binaries having both a separation less than 20 arcsec and a magnitude difference less than 4 mag. Removing these stars results in a list of 120 a priori 'clean' Hyades members (sample 'Hy1'). Solutions starting from this sample are shown in the lower part of Table 3. The results for the Hy1 sample are not significantly different from those of Hy0, except for a smaller velocity dispersion for $g_{\rm lim}$ in the range 15 to 30 (where the selection in Hy1 remains practically the same). This reduction in σ_v is probably real and caused by a smaller proportion of astrometric binaries in sample Hy1.

The Monte Carlo experiments described in Sect. 4.2 suggest that a cut-off limit around $g_{\rm lim} = 15$ might be optimal. Since Hy0 and Hy1 give rather consistent results at this limit, we adopt as the preferred solution the one retaining the larger number of stars, i.e. the one (Hy0, $g_{\rm lim} = 15$) marked with a box in Table 3. In that solution the formal covariance matrix for the three parameters $\widehat{v}_{0x}$, $\widehat{v}_{0y}$, and $\widehat{v}_{0z}$ (the upper-left part of $\boldsymbol{V}_{22}$ in Eq. A.17) is

$$\mathrm{Cov}(\widehat{\boldsymbol{v}}_0) = \begin{bmatrix} 0.01756 & 0.03152 & 0.01120 \\ 0.03152 & 0.11587 & 0.03117 \\ 0.01120 & 0.03117 & 0.01039 \end{bmatrix} \ \mathrm{km^2\ s^{-2}}\,, \quad (23)$$

which however should be multiplied by 1.28^2 to give the actual uncertainties according to Sect. 5.2. We note that the principal axes of the error ellipsoid are nearly aligned (within 8°) with the triad $[\boldsymbol{k}_{\parallel 0}\ \boldsymbol{k}_{\perp 0}\ \boldsymbol{r}_0]$ defined in Appendix A.4 (footnote): the longest axis (corresponding to a velocity uncertainty of 0.37 km s^{-1}) is along the direction $\boldsymbol{r}_0$ toward the cluster centroid; the shortest axis (corresponding to an uncertainty of 0.03 km s^{-1}) is along $\boldsymbol{k}_{\perp 0}$, perpendicular to both $\boldsymbol{r}_0$ and $\boldsymbol{v}_0$.

5.2. Velocity dispersion and error calibration

If the proper-motion residuals from the adopted solution in Table 3 are analysed as described in Sect. 4.3 we find an rms velocity dispersion of $\sigma_\perp = 0.49 \pm 0.04$ km s^{-1} perpendicular to the projected space velocity of the cluster. On the assumption of an isotropic dispersion we take this to be our best estimate of σ_v for the adopted sample of 168 stars. A Monte Carlo simulation with this dispersion accurately reproduces both $\widehat{\sigma}_v$ and the formal errors in Table 3, but the scatter among the solutions also show that the formal errors should be increased by a factor 1.28 to reflect the true uncertainties of the estimates.

As previously mentioned, the distribution of the goodness-of-fit statistics g_i in Fig. 5 indicates a non-Gaussian velocity dispersion with a spread in $\ln\sigma_v$ of the order of $\gamma = 1$. This is however for the original sample of 197 stars, i.e. before the rejection procedure, and the situation may be very different for the final sample of 168 stars. We have investigated the distribution of proper-motion residuals in that sample in order to see if there is evidence for a deviation from a Gaussian velocity dispersion. To this end we generated synthetic samples with Gaussian and other distributions, added random observational errors, and compared the resulting distributions with the observed distribution. Based on the Kolmogorov–Smirnov test (Press et al. 1992), a purely Gaussian velocity dispersion cannot be ruled out. However, a visibly much better agreement

Table 3. Results obtained with real Hipparcos data for the Hyades cluster. ML estimates were calculated, starting both from the full sample (Hy0, 197 stars) and from the reduced sample with only *bona fide* single stars (Hy1, 120 stars). The basic cluster model with $n+4$ parameters was used, and results are given as function of the rejection limit $g_{\rm lim}$. n is the number of stars in the sample after rejection of outliers. $\widehat{\sigma}_v$ is the estimated internal velocity dispersion, and $\widehat{v}_{0x}$, $\widehat{v}_{0y}$, $\widehat{v}_{0z}$, $\widehat{v}_{0r}$ are the estimated components of the centroid space velocity $\boldsymbol{v}_0$ along the equatorial (ICRS) axes and in the radial direction ($\alpha_0 = 66.75^\circ$, $\delta_0 = +16.52^\circ$). Uncertainties ($\pm$) are the formal standard errors in respective solution. The adopted solution, shown in a box, is for the larger sample (Hy0) using the cut-off value $g_{\rm lim} = 15$ indicated as optimal by Monte Carlo simulations. This solution does not include any correction for possible internal velocity field, e.g. representing cluster expansion (see Sect. 5.3). As discussed in Sect. 5.2 our final estimate for the velocity dispersion is $\sigma_v = 0.49 \pm 0.04$ km s^{-1}, while the formal errors on the velocity components need to be multiplied by 1.28.

$g_{\rm lim}$	n	$\widehat{\sigma}_v$	$\widehat{v}_{0x}$	$\widehat{v}_{0y}$	$\widehat{v}_{0z}$	$\widehat{v}_{0r}$	
				[km s^{-1}]			
Solutions starting from sample Hy0:							
∞	197	1.01 ± 0.04	-6.30 ± 0.25	$+45.03 \pm 0.57$	$+5.23 \pm 0.19$	$+38.77 \pm 0.64$	
30	196	0.93 ± 0.04	-5.97 ± 0.24	$+45.69 \pm 0.55$	$+5.44 \pm 0.18$	$+39.53 \pm 0.62$	
25	191	0.76 ± 0.03	-5.84 ± 0.22	$+46.01 \pm 0.51$	$+5.58 \pm 0.16$	$+39.90 \pm 0.56$	
20	171	0.33 ± 0.02	-5.90 ± 0.14	$+45.77 \pm 0.35$	$+5.60 \pm 0.10$	$+39.68 \pm 0.37$	
15	168	0.31 ± 0.02	-5.90 ± 0.13	$+45.65 \pm 0.34$	$+5.56 \pm 0.10$	$+39.56 \pm 0.37$	adopted
10	136	0.08 ± 0.02	-6.05 ± 0.11	$+45.70 \pm 0.31$	$+5.54 \pm 0.08$	$+39.54 \pm 0.32$	
Solutions starting from sample Hy1:							
∞	120	0.96 ± 0.05	-6.45 ± 0.29	$+44.39 \pm 0.65$	$+5.01 \pm 0.22$	$+38.05 \pm 0.72$	
30	110	0.24 ± 0.02	-5.68 ± 0.14	$+46.19 \pm 0.37$	$+5.75 \pm 0.10$	$+40.14 \pm 0.38$	
25	108	0.21 ± 0.02	-5.81 ± 0.13	$+46.18 \pm 0.36$	$+5.69 \pm 0.10$	$+40.06 \pm 0.38$	
20	108	0.21 ± 0.02	-5.81 ± 0.13	$+46.18 \pm 0.36$	$+5.69 \pm 0.10$	$+40.06 \pm 0.38$	
15	107	0.20 ± 0.02	-5.89 ± 0.13	$+45.97 \pm 0.36$	$+5.61 \pm 0.10$	$+39.83 \pm 0.37$	
10	93	0.10 ± 0.03	-6.12 ± 0.13	$+45.73 \pm 0.35$	$+5.53 \pm 0.10$	$+39.51 \pm 0.37$	

was obtained by assuming a log-normal dispersion with median value $\sigma_{v,\rm med} = 0.38 \pm 0.04$ km s^{-1} and $\gamma = 0.5 \pm 0.1$. Roughly speaking, the observed velocity dispersion can thus be interpreted as a mixture of Gaussian distributions, with one third of the stars having a dispersion less than 0.31 km s^{-1}, one third between 0.31 and 0.47 km s^{-1}, and one third greater than 0.47 km s^{-1}. It is tempting to relate this mixture to the range of stellar masses ($\mathcal{M}$) in the sample, where equipartition of energy would require $\sigma_v \propto \mathcal{M}^{-1/2}$. By dividing the sample according to absolute magnitude we do find some positive correlation between M_V and σ_v, but only at a hardly significant $+1.5$ standard deviation. For the solution with $g_{\rm lim} = 15$ starting from sample Hy1, i.e. excluding known binaries, an overall dispersion of 0.37 ± 0.04 km s^{-1} is found, but without visible correlation with M_V. Thus we find no convincing support for the hypothesis that σ_v depends on the stellar mass.

5.3. Cluster expansion

The adopted solution does not take into account effects of a possible systematic velocity pattern within the Hyades cluster. In particular, it assumes that there is no net expansion or contraction of the cluster ($\kappa = 0$). In Paper I it was shown that cluster expansion will bias the astrometric radial-velocity estimate by $\delta_{\rm exp}(v_{ri}) = -b_i\kappa$, where b_i is the distance to the star and κ the expansion rate. If the expansion rate of the Hyades cluster equals the inverse cluster age, then $\delta_{\rm exp} \simeq -0.07$ km s^{-1}. However, at least the inner part of the Hyades cluster is gravitationally bound, and so is not expected to expand. The actual state of the cluster in terms of expansion or contraction is essentially unknown and may depend on the selection of stars. We have therefore chosen *not* to apply any corresponding correction to the data in Table 3.

5.4. Spatial correlations

One further approximation in the present method needs to be discussed. It concerns our neglecting the possible correlations among the astrometric data for different stars [Eq. (9)]. It is well known that the observational technique used by Hipparcos tends to give positive correlations among the data for stars within an area of the sky comparable with the instrument's field of view, $\sim 1^\circ$ (Lindegren 1988; ESA 1997, Vol. 3, Ch. 16–17). The degree of correlation in the Hipparcos data and the extent to which it affects e.g. the determination of cluster distances is however controversial (Narayanan & Gould 1999b; van Leeuwen 1999a). In the case of the Hyades cluster, the parallax residuals from the adopted ML solution make it possible to obtain a rough estimate of the spatial correlations, since these residuals are dominated by the parallax errors in the Hipparcos Catalogue. We made a correlation analysis of the normalised residuals $(\widetilde{\pi}_i - \widehat{\pi}_i)/\epsilon(\widetilde{\pi}_i)$ as function of the angular separation between stars. The normalisation was made in order to get roughly equal weight to the residuals. For pairs with separation in the intervals 0–0.5°, 0.5–1.0° and 1–2°, we found the sample correlation coefficients $+0.13 \pm 0.11$, $+0.12 \pm 0.07$, and -0.01 ± 0.03, respectively.

The positive values for separations $< 1^\circ$ depend on a small number of pairs involving the two stars HIP 19834 and 19862, both of which have strong positive residuals ($+10.67 \pm 3.74$ and $+9.32 \pm 2.76$ mas), but which are otherwise unremarkable. If a more robust estimator is used, such as the median product of the residuals, then no correlation at all is found at these separations. We conclude that the spatial correlations, if they exist, are probably less than $+0.15$, with a range of about 1°. Similar correlations were found by van Leeuwen (1999b).

Unless these correlations are included in the observation model, or in the simulations, it is difficult to assess how they would affect the solution. Probably, the main effect of their omission is that the errors of the solution are underestimated, similar to the case for the mean parallax of a cluster (Lindegren 1988). However, the moving-cluster method depends on the determination of proper-motion *gradients* across a cluster, and these first moments are generally much less sensitive to local correlations than are the zeroth moments (e.g. the mean parallax). For instance, if we assume that the correlation in the Hyades cluster is $+0.15$ for separations up to 1°, and zero otherwise, then the standard error of the mean parallax may be underestimated by as much as 19 per cent, while the standard errors of the gradients are only underestimated by 1.5 to 4 per cent (along α and δ, respectively, assuming the spatial distribution of the final sample of 168 stars). We therefore conclude that the effects of the correlations on the ML solution are relatively small for very extended objects such as the Hyades and nearby OB associations, the only objects for which the method is expected to yield significant results with Hipparcos data. Neglecting the correlations should therefore be a reasonable first approximation in our applications of the method.

A more complete treatment of the correlations will in practice require the present ML solution to be re-formulated along the principles described by van Leeuwen & Evans (1998), i.e. by treating the Hipparcos Intermediate Astrometric Data (ESA 1997, Vol. 17, Disk 5) as (correlated) observations, instead of the catalogued parallax and proper-motion values. Such an exercise is however beyond the scope of this paper.

6. Conclusions

We have developed and implemented a rigorous maximum-likelihood algorithm for estimating the kinematic parameters of an open cluster or association from astrometric data, i.e. without using spectroscopic information. The cluster parameters comprise, in the basic model, the individual distances to the stars, the centroid space velocity vector and the internal velocity dispersion. Extended models include cluster rotation and other components of a first-order systematic velocity field, except the isotropic dilation (expansion or contraction) which cannot be determined purely by astrometry. From the estimated cluster parameters, the radial velocities of the individual stars are obtained independent of spectroscopic data. The solution also provides kinematically improved parallaxes for the individual stars.

Extensive Monte Carlo simulations have been used to test the ML algorithm and its statistical properties. The main conclusions are (1) that the basic kinematic parameters are estimated without significant bias, except for the internal velocity dispersion, which is normally underestimated; (2) that a sequential rejection procedure based on the goodness-of-fit statistics g_i is effective in eliminating otherwise contaminating outliers such as caused by astrometric binaries or non-member stars; (3) that a posteriori analysis of the proper motion residuals yields an improved (nearly unbiased) estimate of the internal velocity dispersion; and (4) that Monte Carlo simulations are essential for validating the model assumptions and for providing realistic confidence limits for the estimated parameters.

In this paper the method has been applied to the Hyades. On the assumption that the cluster has no net expansion or contraction, we find the centroid space velocity $\boldsymbol{v}_0 = (-5.90 \pm 0.17, +45.65 \pm 0.44, +5.56 \pm 0.13)$ km s^{-1}, where the uncertainties have been corrected by the factor 1.28 derived in Sect. 5.2. The covariance of this estimate is given by Eq. (23) multiplied by 1.28^2. The internal velocity dispersion for the adopted sample of 168 stars is estimated at $\sigma_v = 0.49 \pm 0.04$ km s^{-1}, although the distribution of proper-motion residuals suggests a slightly non-Gaussian velocity distribution. This could be characterised as a log-normal spread of dispersions having a median value $\sigma_{v,\mathrm{med}} = 0.38$ km s^{-1} and $\gamma = 0.5$. The resulting astrometric radial velocities have a (position-dependent) uncertainty of about 0.68 km s^{-1} for the individual values and 0.47 km s^{-1} for the centroid radial velocity. The greater errors for the individual radial velocities arise from quadratically adding the radial uncertainty of the stellar peculiar velocities (0.49 km s^{-1}) to that of the projected centroid velocity. If known binaries are removed, a smaller dispersion of 0.37 km s^{-1} is found, corresponding to a standard error of 0.60 km s^{-1} for the individual radial velocities.

The distributions of g_i values (Fig. 5) contain evidence for a much more strongly non-Gaussian velocity distribution in the original sample of 197 stars. Possible effects of internal velocity fields are further addressed in the subsequent Paper III, in which this method will be applied also to other nearby clusters and associations.

Acknowledgements. This project is supported by the Swedish National Space Board and the Swedish Natural Science Research Council. We thank the referee, Dr. Andrew Gould (Ohio State University), for stimulating criticism and constructive suggestions.

Appendix A: Implementation of the maximum-likelihood solution

A.1. Observational data

The most promising star clusters and associations for the determination of astrometric radial velocities are identified in Table 3 of Paper I. Using astrometric data from the Hipparcos Catalogue (ESA 1997), solutions for some of these clusters will be discussed in Paper III. Here we identify the data items in the

Hipparcos Catalogue that are required as input to the computations.

For each star (i) the main observational data required are the trigonometric parallax $\widetilde{\pi}_i$ and the proper motion components $\widetilde{\mu}_{\alpha i}$ and $\widetilde{\mu}_{\delta i}$. These may be taken directly from Fields H11–13 of the Hipparcos Catalogue and define the arrays $\widetilde{\boldsymbol{a}}_i$ [cf. Eq. (6)]. The standard errors of the observables $\epsilon(\pi_i)$, $\epsilon(\mu_{\alpha*i})$ and $\epsilon(\mu_{\delta i})$ are given in Fields H16–18 of the catalogue. These are used together with the correlation coefficients $\rho(\pi_i, \mu_{\alpha*i})$ (Field H24), $\rho(\pi_i, \mu_{\delta i})$ (H27) and $\rho(\mu_{\alpha*i}, \mu_{\delta i})$ (H28) to compute the 3×3 covariance matrix $\boldsymbol{C}_i$. The elements are

$$\begin{aligned}
&[\boldsymbol{C}_i]_{11} = \epsilon(\pi_i)^2 \,, \\
&[\boldsymbol{C}_i]_{12} = [\boldsymbol{C}_i]_{21} = \epsilon(\pi_i)\epsilon(\mu_{\alpha*i})\rho(\pi_i, \mu_{\alpha*i}) \,, \\
&[\boldsymbol{C}_i]_{13} = [\boldsymbol{C}_i]_{31} = \epsilon(\pi_i)\epsilon(\mu_{\delta i})\rho(\pi_i, \mu_{\delta i}) \,, \\
&[\boldsymbol{C}_i]_{22} = \epsilon(\mu_{\alpha*i})^2 \,, \\
&[\boldsymbol{C}_i]_{23} = [\boldsymbol{C}_i]_{32} = \epsilon(\mu_{\alpha*i})\epsilon(\mu_{\delta i})\rho(\mu_{\alpha*i}, \mu_{\delta i}) \,, \\
&[\boldsymbol{C}_i]_{33} = \epsilon(\mu_{\delta i})^2 \,.
\end{aligned} \tag{A.1}$$

Units are the milliarcsec (mas) for the parallax, mas yr^{-1} for the proper motion components (where 1 yr is exactly 365.25 days), and km s^{-1} for linear velocities. In this system the astronomical unit is $A \simeq 4.74047$ km yr s^{-1}.

The normal triad $[\boldsymbol{p}_i \;\; \boldsymbol{q}_i \;\; \boldsymbol{r}_i]$ introduced in Sect. 3.4 is computed from the right ascension α_i and declination δ_i in Fields H8–9 of the Hipparcos Catalogue. The equatorial Cartesian components of these vectors are

$$\begin{aligned}
\boldsymbol{p}_i &= \begin{bmatrix} -\sin\alpha_i \\ \cos\alpha_i \\ 0 \end{bmatrix} , \quad \boldsymbol{q}_i = \begin{bmatrix} -\sin\delta_i\cos\alpha_i \\ -\sin\delta_i\sin\alpha_i \\ \cos\delta_i \end{bmatrix} , \\
\boldsymbol{r}_i &= \begin{bmatrix} \cos\delta_i\cos\alpha_i \\ \cos\delta_i\sin\alpha_i \\ \sin\delta_i \end{bmatrix} .
\end{aligned} \tag{A.2}$$

A.2. Solution of the maximum-likelihood equations

The ML estimate $\widehat{\boldsymbol{\theta}}$ is obtained by finding the maximum of $\mathcal{L}(\boldsymbol{\theta})$, or, equivalently, the minimum of $U(\boldsymbol{\theta})$ in Eq. (18). Standard numerical packages for non-linear minimisation can be used to achieve this more or less efficiently. Since many thousand minimisations are required in the Monte Carlo simulations, it is not without interest to have a computationally efficient implementation. We have found that a standard Newton–Raphson iterative method performs very well if advantage is taken of the sparse structure of the linearised equations, as described below. A complete minimisation for $n \sim 10^2$ stars takes a fraction of a second on a standard PC, and the time grows only linearly with n.

Recall that the dimension of $\boldsymbol{\theta}$ is $m = n + 4$ for the basic cluster model, and $m = n + 7$ or $n + 12$ for the models including systematic velocity patterns (Sect. 3.3). Define the m-dimensional function $\boldsymbol{f}(\boldsymbol{\theta}) \equiv \partial\mathcal{L}/\partial\boldsymbol{\theta}$ so that $\boldsymbol{f}(\boldsymbol{\theta}) = \boldsymbol{0}$ is a system of non-linear equations to be solved. In the Newton–Raphson iterative method (Press et al. 1992, Ch. 9.6) an improvement $\Delta\boldsymbol{\theta}$ to the current approximation $\boldsymbol{\theta}$ is obtained by solving the linearised equations $\boldsymbol{f}(\boldsymbol{\theta} + \Delta\boldsymbol{\theta}) \simeq \boldsymbol{f}(\boldsymbol{\theta}) + (\partial\boldsymbol{f}/\partial\boldsymbol{\theta}')\Delta\boldsymbol{\theta} = \boldsymbol{0}$. Writing $\boldsymbol{H}(\boldsymbol{\theta}) = \partial^2\mathcal{L}/\partial\boldsymbol{\theta}\partial\boldsymbol{\theta}'$ for the Hessian matrix the improvement is therefore $\Delta\boldsymbol{\theta} = -\boldsymbol{H}(\boldsymbol{\theta})^{-1}\boldsymbol{f}(\boldsymbol{\theta})$. This equation is iterated until $|\Delta\boldsymbol{\theta}|$ is negligible. While $\boldsymbol{f}(\boldsymbol{\theta})$ must of course be calculated rigorously in order that the final $\boldsymbol{\theta}$ should represent the true ML solution, it is possible to use various approximations in the calculation of $\boldsymbol{H}$, as long as the procedure converges. In fact, it is usually advantageous to neglect the terms in $\boldsymbol{H}$ that depend linearly on the residuals (Press et al. 1992, Ch. 15.5). Thus, we introduce the $m \times m$ matrix $\boldsymbol{N} \equiv -\mathrm{E}(\boldsymbol{H})$, also required for estimating the covariance of the ML estimate according to Eq. (1). The system to be solved in each iteration is then $\boldsymbol{N} \cdot \Delta\boldsymbol{\theta} = \boldsymbol{f}$.

With $f_j = \partial\mathcal{L}/\partial\theta_j$, $d_i = |\boldsymbol{D}_i|$ and $\boldsymbol{G}_i = \boldsymbol{D}_i^{-1}$ we have from Eq. (17)

$$\begin{aligned}
f_j = \sum_{i=1}^{n} \Bigg[&\sum_{\alpha=1}^{3}\sum_{\beta=1}^{3} G_{i\alpha\beta}\frac{\partial c_{i\alpha}}{\partial\theta_j}(\widetilde{a}_{i\beta} - c_{i\beta}) - \frac{1}{2}\frac{\partial \ln d_i}{\partial\theta_j} \\
&- \frac{1}{2}\sum_{\alpha=1}^{3}\sum_{\beta=1}^{3}\frac{\partial G_{i\alpha\beta}}{\partial\theta_j}(\widetilde{a}_{i\alpha} - c_{i\alpha})(\widetilde{a}_{i\beta} - c_{i\beta}) \Bigg]
\end{aligned} \tag{A.3}$$

for $j = 1 \ldots m$. Differentiating a second time, now with respect to θ_k, $k = 1 \ldots m$, and using that $\mathrm{E}(\widetilde{a}_{i\alpha} - c_{i\alpha}) = 0$ and $\mathrm{E}[(\widetilde{a}_{i\alpha} - c_{i\alpha})(\widetilde{a}_{i\beta} - c_{i\beta})] = D_{i\alpha\beta}$, we find

$$\begin{aligned}
N_{jk} = \sum_{i=1}^{n} \Bigg[&\sum_{\alpha=1}^{3}\sum_{\beta=1}^{3} G_{i\alpha\beta}\frac{\partial c_{i\alpha}}{\partial\theta_j}\frac{\partial c_{i\beta}}{\partial\theta_k} + \frac{1}{2}\frac{\partial^2 \ln d_i}{\partial\theta_j\partial\theta_k} \\
&+ \frac{1}{2}\sum_{\alpha=1}^{3}\sum_{\beta=1}^{3} D_{i\alpha\beta}\frac{\partial^2 G_{i\alpha\beta}}{\partial\theta_j\partial\theta_k} \Bigg] .
\end{aligned} \tag{A.4}$$

The main complication in solving the ML equations arises because $\boldsymbol{D}_i$ depends on the model parameters π_i and σ_v through Eq. (16); hence the second and third terms on the right-hand sides of Eqs. (A.3) and (A.4). Fortunately the structure of $\boldsymbol{D}_i$ allows considerable simplification of the calculations. We note that the dependence on π_i and σ_v is only through the variable $e_i = (\pi_i\sigma_v/A)^2$. Writing Eq. (16) as $\boldsymbol{D}_i = \boldsymbol{C}_i + \boldsymbol{P}e_i$, where $\boldsymbol{P} = \mathrm{diag}(0, 1, 1)$, we find by direct expansion of the determinant

$$\frac{\partial \ln d_i}{\partial e_i} = G_{i22} + G_{i33} \,, \tag{A.5}$$

from which the second term in Eq. (A.3) can be calculated. Using the Woodbury formula (Press et al. 1992) we also find

$$\frac{\partial \boldsymbol{G}_i}{\partial e_i} = -\boldsymbol{G}_i\boldsymbol{P}\boldsymbol{G}_i \,, \tag{A.6}$$

from which the third term in Eq. (A.3) is obtained. Application of the last two formulae to the second and third terms in Eq. (A.4) gives:

$$\begin{aligned}
N_{jk} = \sum_{i=1}^{n} \Bigg[&\sum_{\alpha=1}^{3}\sum_{\beta=1}^{3} G_{i\alpha\beta}\frac{\partial c_{i\alpha}}{\partial\theta_j}\frac{\partial c_{i\beta}}{\partial\theta_k} \\
&+ \frac{1}{2}(G_{i22}^2 + 2G_{i23}^2 + G_{i33}^2)\frac{\partial e_i}{\partial\theta_j}\frac{\partial e_i}{\partial\theta_k} \Bigg] .
\end{aligned} \tag{A.7}$$

The matrix $\boldsymbol{N}$ is symmetric and, if all the parameters are estimable, positive definite. Thus a wide range of numerical methods are available to solve the system $\boldsymbol{N}\cdot\Delta\boldsymbol{\theta}=\boldsymbol{f}$ and to compute the inverse matrix $\boldsymbol{V}=\boldsymbol{N}^{-1}$ for Eq. (1). Efficient implementations should however take advantage of the sparse structure of $\boldsymbol{N}$: it contains non-zero elements only along the diagonal and in a border of width $m-n$ along the right and bottom edges. The system of equations may be partitioned

$$\begin{array}{c} \\ n \\ m-n \end{array} \begin{array}{c} \begin{array}{cc} n & m-n \end{array} \\ \begin{bmatrix} \boldsymbol{N}_{11} & \boldsymbol{N}_{12} \\ \boldsymbol{N}_{21} & \boldsymbol{N}_{22} \end{bmatrix} \end{array} \begin{array}{c} \begin{array}{c} 1 \end{array} \\ \begin{bmatrix} \Delta\boldsymbol{\theta}_1 \\ \Delta\boldsymbol{\theta}_2 \end{bmatrix} \end{array} = \begin{array}{c} \begin{array}{c} 1 \end{array} \\ \begin{bmatrix} \boldsymbol{f}_1 \\ \boldsymbol{f}_2 \end{bmatrix} \end{array}, \tag{A.8}$$

where the dimensions of the submatrices are indicated above and to the left of the system. $\boldsymbol{N}_{11}$ is diagonal and therefore its inversion is trivial. With this in mind we can eliminate $\Delta\boldsymbol{\theta}_1$ to obtain a system of dimension $m-n$,

$$(\boldsymbol{N}_{22}-\boldsymbol{N}_{21}\boldsymbol{N}_{11}^{-1}\boldsymbol{N}_{12})\Delta\boldsymbol{\theta}_2=\boldsymbol{f}_2-\boldsymbol{N}_{21}\boldsymbol{N}_{11}^{-1}\boldsymbol{f}_1\,, \tag{A.9}$$

from which $\Delta\boldsymbol{\theta}_2$ is solved. Back-substitution then gives

$$\Delta\boldsymbol{\theta}_1=\boldsymbol{N}_{11}^{-1}(\boldsymbol{f}_1-\boldsymbol{N}_{12}\Delta\boldsymbol{\theta}_2)\,. \tag{A.10}$$

For fixed $m-n$ the number of operations required to solve this system grows linearly with the number of stars (n).

A.3. Standard errors of the estimated quantities

After convergence to the ML estimate $\widehat{\boldsymbol{\theta}}$, elements of the covariance matrix $\boldsymbol{V}=\boldsymbol{N}^{-1}$ may be computed after partitioning in analogy with Eq. (A.8). The covariance of the cluster parameters $\widehat{\boldsymbol{\theta}}_2\equiv(\widehat{\boldsymbol{v}}_0,\widehat{\sigma}_v,\ldots)$ is thus found to be

$$\boldsymbol{V}_{22}=(\boldsymbol{N}_{22}-\boldsymbol{N}_{21}\boldsymbol{N}_{11}^{-1}\boldsymbol{N}_{12})^{-1}\,, \tag{A.11}$$

from which the covariance of $\widehat{\boldsymbol{\theta}}_1\equiv\widehat{\boldsymbol{\pi}}$ is obtained as

$$\boldsymbol{V}_{11}=\boldsymbol{N}_{11}^{-1}+\boldsymbol{N}_{11}^{-1}\boldsymbol{N}_{12}\boldsymbol{V}_{22}\boldsymbol{N}_{21}\boldsymbol{N}_{11}^{-1}\,. \tag{A.12}$$

The remaining parts of $\boldsymbol{V}$ are

$$\boldsymbol{V}_{12}=\boldsymbol{V}_{21}'=-\boldsymbol{N}_{11}^{-1}\boldsymbol{N}_{12}\boldsymbol{V}_{22}\,. \tag{A.13}$$

The standard errors of the estimated parameters are computed from the diagonal elements of $\boldsymbol{V}$:

$$\epsilon(\widehat{\theta}_j)^2=V_{jj}\,. \tag{A.14}$$

More generally, the standard error of any quantity which is a function of the estimated model parameters, say $\widehat{z}\equiv z(\widehat{\boldsymbol{\theta}})$, is computed from

$$\epsilon(\widehat{z})^2=\frac{\partial z}{\partial\boldsymbol{\theta}'}\,\boldsymbol{V}\,\frac{\partial z}{\partial\boldsymbol{\theta}}\,. \tag{A.15}$$

For instance, the estimated radial velocity of the cluster centroid is given by the projection of $\widehat{\boldsymbol{v}}_0$ along the direction to the centroid, $\boldsymbol{r}_0=\boldsymbol{b}_0/|\boldsymbol{b}|_0$,

$$\widehat{v}_{0r}=\boldsymbol{r}_0'\widehat{\boldsymbol{v}}_0\,, \tag{A.16}$$

and its standard error (in the basic cluster model) is therefore given by

$$\epsilon(\widehat{v}_{0r})^2=[\,r_{0x}\;r_{0y}\;r_{0z}\;0\,]\,\boldsymbol{V}_{22}\begin{bmatrix} r_{0x}\\ r_{0y}\\ r_{0z}\\ 0\end{bmatrix}\,. \tag{A.17}$$

For the radial-velocity estimates of the individual stars, computed according to Eq. (20), the contribution from the radial component of the star's peculiar velocity must however also be taken into account. To sufficient approximation the formula

$$\epsilon(\widehat{v}_{ri})^2=[\,r_{xi}\;r_{xi}\;r_{zi}\;0\,]\,\boldsymbol{V}_{22}\begin{bmatrix} r_{xi}\\ r_{yi}\\ r_{zi}\\ 0\end{bmatrix}+\sigma_v^2 \tag{A.18}$$

may be used. For σ_v the estimated value corrected for bias should be used, or (better) the value estimated from proper motion residuals according to Appendix A.4. It should be noted that the individual radial-velocity errors in a given cluster are strongly correlated due to the common error resulting from the estimated centroid velocity.

A.4. Velocity dispersion estimated from residuals

As discussed in Sect. 4.3, the velocity dispersion of the cluster (σ_v) can be estimated from an analysis of the proper-motion residuals perpendicular to the centroid velocity projected on the sky. For each star (i) we defined the normal triad $[\boldsymbol{p}_i\;\boldsymbol{q}_i\;\boldsymbol{r}_i]$ through Eq. (A.2). Having determined the centroid velocity $\boldsymbol{v}_0$ by means of the ML solution, we can now define the supplementary triad $[\boldsymbol{k}_{\parallel i}\;\boldsymbol{k}_{\perp i}\;\boldsymbol{r}_i]$, where

$$\boldsymbol{k}_{\perp i}=(\boldsymbol{r}_i\times\widehat{\boldsymbol{v}}_0)|\boldsymbol{r}_i\times\widehat{\boldsymbol{v}}_0|^{-1}\,,\quad \boldsymbol{k}_{\parallel i}=\boldsymbol{r}_i\times\boldsymbol{k}_{\perp i} \tag{A.19}$$

are unit vectors in the plane of the sky, oriented perpendicular and parallel to the plane containing the observer, the star, and $\widehat{\boldsymbol{v}}_0$.[4] The proper motion residuals from the ML solution are contained in the vectors $\widetilde{\boldsymbol{a}}_i-\widehat{\boldsymbol{a}}_i$. Introducing the auxiliary vector

$$\boldsymbol{h}_i=[0\;\boldsymbol{p}_i\;\boldsymbol{q}_i]'\boldsymbol{k}_{\perp i} \tag{A.20}$$

we compute the peculiar velocities in the $\perp$ direction as

$$\eta_{\perp i}=(A/\widehat{\pi}_i)\boldsymbol{h}_i'(\widetilde{\boldsymbol{a}}_i-\widehat{\boldsymbol{a}}_i)\,, \tag{A.21}$$

and their uncertainties as

$$\epsilon(\eta_{\perp i})=(A/\widehat{\pi}_i)(\boldsymbol{h}_i'\boldsymbol{C}_i\boldsymbol{h}_i)^{1/2}\,. \tag{A.22}$$

In the latter expression, only the proper-motion errors are taken into account.

To estimate the true velocity dispersion, we use the ML method with $\eta_{\perp i}$ regarded as independent observations of a

[4] Narayanan & Gould (1999a) discuss Hyades data in a similar coordinate system, but oriented with respect to the centroid direction $\boldsymbol{r}_0$ (i.e. the same axis directions are used for all the stars). In our notation, that triad could be designated $[\boldsymbol{k}_{\parallel 0}\;\boldsymbol{k}_{\perp 0}\;\boldsymbol{r}_0]$.

Gaussian population with mean value zero and standard deviation $\sigma_\perp$. Each observation has the standard error $\epsilon(\eta_{\perp i})$. The required estimate $\widehat{\sigma}_\perp$ is obtained by solving the non-linear equation

$$F(\sigma_\perp) \equiv \sum_{i=1}^{n} \frac{\eta_{\perp i}^2 - \sigma_\perp^2 - \epsilon(\eta_{\perp i})^2}{[\sigma_\perp^2 + \epsilon(\eta_{\perp i})^2]^2} = 0\,. \qquad \text{(A.23)}$$

[This equation has no solution if $F(0) < 0$, which corresponds to an rms proper-motion residual smaller than that expected from the observational uncertainties. In that case we set $\widehat{\sigma}_\perp = 0$.] The uncertainty of the estimate, obtained by means of Eq. (1), is given by

$$\epsilon(\widehat{\sigma}_\perp) = \left[2\widehat{\sigma}_\perp^2 \sum_{i=1}^{n} [\widehat{\sigma}_\perp^2 + \epsilon(\eta_{\perp i})^2]^{-2} \right]^{-1/2} . \qquad \text{(A.24)}$$

Appendix B: Notations

This Appendix summarises notations used in this paper. Equation numbers refer to the place where the notation is defined or first used.

Lower-case bold-face letters designate vectors and arrays, upper-case bold-face letters tensors and matrices. Ordinary-face italics are used for scalar variables. The prime ($'$) denotes the transpose of a matrix as well as the scalar product of vectors. For the generic variable x the true value is designated $\overline{x}$, the observed value $\widetilde{x}$ and the estimated value $\widehat{x}$. $\epsilon(x)$ is the uncertainty (standard error) of x, $\langle x \rangle$ the sample mean value and $\mathrm{E}(x)$ the expectation. $\mathrm{Cov}(\boldsymbol{x}) \equiv \mathrm{E}[\{\boldsymbol{x} - \mathrm{E}(\boldsymbol{x})\}\{\boldsymbol{x} - \mathrm{E}(\boldsymbol{x})\}']$ is the covariance operator. $\rho(x, y)$ is the statistical correlation (from -1 to $+1$) between x and y. Pr denotes probability.

A	$= 4.74047\ldots$ km yr s^{-1}, the astronomical unit
$\boldsymbol{a}$	vector of astrometric observables for all stars
$\boldsymbol{a}_i$	vector of astrometric observables for star i (6)
$\boldsymbol{b}_0$	position of the cluster centroid relative the Sun
$\boldsymbol{b}_i$	position of star i relative the Sun
$\boldsymbol{C}_i$	covariance of observational errors in $\boldsymbol{a}_i$ (8)
$\boldsymbol{c}_i$	expectation of $\boldsymbol{a}_i$ according to model (15)
$\boldsymbol{D}_i$	covariance of $\boldsymbol{a}_i$ including velocity dispersion (16)
$\boldsymbol{f}$	vector of partial derivatives $f_j = \partial\mathcal{L}/\partial\theta_j$
$\boldsymbol{G}_i$	the inverse of $\boldsymbol{D}_i$
g_i	goodness-of-fit statistic for star i (19)
$g_{\lim}$	rejection limit for g_i (22)
$\boldsymbol{H}$	Hessian matrix of second-order partial derivatives $H_{jk} = \partial^2\mathcal{L}/\partial\theta_j\partial\theta_k$
i	$= 1\ldots n$, star index
j	$= 1\ldots m$, parameter index
$\boldsymbol{k}_{\parallel i}$	unit vector in the plane of the sky parallel to the projected space velocity of the cluster (A.19)
$\boldsymbol{k}_{\perp i}$	unit vector in the plane of the sky perpendicular to the projected space velocity of the cluster (A.19)
$\mathcal{L}$	$= \ln L$, log-likelihood (17)
m	total number of model parameters
$\boldsymbol{N}$	$= -\mathrm{E}(\boldsymbol{H})$, the $m \times m$ normal matrix (A.4)
n	number of stars in the cluster
p	probability density functions (5,10,12,13)
$\boldsymbol{p}_i$	unit vector towards local 'East' at star i (A.2)
$\boldsymbol{q}_i$	unit vector towards local 'North' at star i (A.2)
$\boldsymbol{r}_i$	unit vector towards star i (A.2)
$\boldsymbol{S}$	internal velocity dispersion tensor (2)
$\boldsymbol{T}$	tensor describing a linear velocity field (3)
$\boldsymbol{u}_i$	expected space velocity of star i (3)
$\boldsymbol{V}$	$= \boldsymbol{N}^{-1}$, estimated covariance of the parameters (1)
$\boldsymbol{v}_0$	space velocity of the cluster centroid
$\boldsymbol{v}_i$	space velocity of star i
v_{0r}	radial velocity of cluster centroid
v_{ri}	radial velocity of star i
$\boldsymbol{w}$	vector describing anisotropic dilation of cluster (4)
x, y, z	Cartesian components in the equatorial system
α_i	right ascension of star i (A.2)
β	empirical scaling factor for g_i (21)
γ	width of the log-normal distribution of σ_v, Sect. 4.2
δ_i	declination of star i (A.2)
$\boldsymbol{\eta}_i$	peculiar space velocity of star i, Sect. 3.3
$\eta_{\parallel i}, \eta_{\perp i}$	components of $\boldsymbol{\eta}_i$ along $\boldsymbol{k}_{\parallel i}$ and $\boldsymbol{k}_{\perp i}$
$\boldsymbol{\theta}$	vector of all m model parameters
θ_j	jth model parameter in $\boldsymbol{\theta}$
κ	cluster expansion rate, Sect. 3.3
$\mu_{\alpha* i}$	proper motion component in right ascension for star i (including $\cos\delta_i$ factor)
$\mu_{\delta i}$	proper motion component in declination for star i
Π	$= 3.1415\ldots$
$\boldsymbol{\pi}$	vector of all n parallaxes
π_i	parallax for star i
σ_v	internal velocity dispersion per coordinate
$\sigma_\perp$	internal velocity dispersion along $\boldsymbol{k}_{\perp i}$
$\boldsymbol{\omega}$	angular velocity of the cluster (4)

References

Binney J., Merrifield M., 1998, Galactic Astronomy. Princeton University Press, Princeton

Casella G., Berger R.L., 1990, Statistical Inference. Duxbury Press, Belmont

de Bruijne J.H.J., 1999, MNRAS 310, 585

Dravins D., Lindegren L., Madsen S., 1999, A&A 348, 1040 (Paper I)

Dravins D., Lindegren L., Madsen S., Holmberg J., 1997, In: Perryman M.A.C., Bernacca P.L. (eds.) Hipparcos Venice '97, ESA SP-402, p. 733

ESA, 1997, The Hipparcos and Tycho Catalogues. ESA SP–1200

Griffin R.F., Griffin R.E.M., Gunn J.E., Zimmerman B.A., 1988, AJ 96, 172

Gunn J.E., Griffin R.F., Griffin R.E.M., Zimmerman B.A., 1988, AJ 96, 198

Hawley S.L., Jefferys W.H., Barnes T.G. III, Lai W., 1986, ApJ 302, 626

Kendall M., Stuart A., 1979, The Advanced Theory of Statistics. Vol. 2: Inference and relationships (4th ed.). Charles Griffin, London

Lindegren L., 1988, In: Torra J., Turon C. (eds.) The European Astrometry Satellite Hipparcos. Scientific Aspects of the Input Catalogue Preparation II, Proc. Coll. Sitges, p. 179

Lindegren L., Dravins D., Madsen S., 1999, In: Hearnshaw J.B., Scarfe C.D. (eds.) Precise Stellar Radial Velocities. ASPC No. 185, IAU Coll. 170, p. 73
Madsen S., 1999, In: Egret D., Heck A. (eds.) Harmonizing Cosmic Distance Scales in a Post-Hipparcos Era. ASPC No. 167, p. 78
Murray C.A., 1983, Vectorial Astrometry. Adam Hilger, Bristol
Murray C.A., Harvey G.M., 1976, Royal Greenwich Obs. Bull. 182, 15
Narayanan V.K., Gould A., 1999a, ApJ 515, 256
Narayanan V.K., Gould A., 1999b, ApJ 523, 328
Perryman M.A.C., Brown A.G.A., Lebreton Y., et al., 1998, A&A 331, 81
Platais I., Kozhurina-Platais V., van Leeuwen F., 1998, AJ 116, 2423
Popowski P., Gould A., 1998, ApJ 506, 259
Press W.H., Teukolsky S.A., Vetterling W.T., Flannery B.P., 1992, Numerical Recipes (2nd ed.). Cambridge Univ. Press, Cambridge
Silvey S.D., 1970, Statistical Inference. Penguin Books, Harmondsworth
Strugnell P., Reid N., Murray C.A., 1986, MNRAS 220, 413
van Bueren H.G., 1952, Bull. Astron. Inst. Netherlands 11, 385
van Leeuwen F., 1999a, A&A 341, L71
van Leeuwen F., 1999b, In: Egret D., Heck A. (eds.) Harmonizing Cosmic Distance Scales in a Post-Hipparcos Era. ASPC No. 167, p. 52
van Leeuwen F., Evans D.W., 1998, A&AS 130, 157